mathematics

Article

Metaheuristic Procedures for the Determination of a Bank of Switching Observers toward Soft Sensor Design with Application to an Alcoholic Fermentation Process

Nikolaos D. Kouvakas [1], Fotis N. Koumboulis [1], Dimitrios G. Fragkoulis [1] and George F. Fragulis [2,*]

[1] Robotics, Automatic Control and Cyber-Physical Systems Laboratory, Department of Digital Industry Technologies, School of Science, National and Kapodistrian University of Athens, Euripus Campus, 34400 Euboea, Greece; nkouvak@dind.uoa.gr (N.D.K.); fkoumboulis@dind.uoa.gr (F.N.K.); dfragkoulis@uoa.gr (D.G.F.)
[2] Internet of Things and Applications Lab, Department of Electrical and Computer Engineering, University of Western Macedonia, 50100 Kozani, Greece
* Correspondence: gfragulis@uowm.gr

Abstract: The present work focused on the development of soft sensors for single-input single-output (SISO) nonlinear dynamic systems with unknown physical parameters using a switching observer design. Toward the development of more accurate soft sensors, as compared with hard sensors, an extended design methodology for the determination of a bank of operating points satisfying the dense web principle was proposed, where for the determination of the bank of operating points and the observer parameters, a metaheuristic procedure was developed. To validate the results of the metaheuristic algorithm, the case of an alcoholic fermentation process was studied as a special case of the present approach. For the nonlinear model of the process, an observer-based soft sensor was developed using the metaheuristic procedure. First, the accuracy of the linear approximant of the process with respect to the original nonlinear model was investigated. Second, the I/O reconstructability of the linear approximant was verified. Third, based on the linear approximant, an observer was designed for the estimation of the non-measurable variable. Fourth, considering that the observer is designed upon the linear approximant, the linear approximant model parameters are derived through identification, for different operating points, upon the nonlinear model. Fifth, the observers corresponding to the different operating points, constitute a bank of observers. The design was completed using a data-driven rule-based system, performing stepwise switching between the observers of the bank. The efficiency of the proposed metaheuristic algorithm and the performance of the switching scheme were demonstrated through a series of computational experiments, where it was observed that the herein-proposed approach was more than two orders of magnitude more accurate than traditional single-step approaches of transition from one operating point to another.

Keywords: metaheuristic algorithms; alcoholic fermentation; soft sensors; switching observers

MSC: 93C41

check for updates

Citation: Kouvakas, N.D.; Koumboulis, F.N.; Fragkoulis, D.G.; Fragulis, G.F. Metaheuristic Procedures for the Determination of a Bank of Switching Observers toward Soft Sensor Design with Application to an Alcoholic Fermentation Process. *Mathematics* **2023**, *11*, 4733. https://doi.org/10.3390/math11234733

Academic Editor: Zhanybai T. Zhusubaliyev

Received: 16 October 2023
Revised: 13 November 2023
Accepted: 20 November 2023
Published: 22 November 2023

1. Introduction

Despite the multitude of advantages of the use of soft sensing schemes, one of the major issues toward their design and implementation is the highly nonlinear nature of the modes of the process or, in several cases, the inherent switching nature of the systems. Toward alleviating these types of difficulties, several approaches have been proposed in the literature for either the observer design or the familiar controller design problem. Indicatively, see [1–7] and the references therein. Switching observers are particularly useful in systems where mode changes or nonlinear variations significantly impact the system's behavior. In such systems, it is essential to have accurate state estimation that contributes to maintaining control and stability. By using switching observers, control systems can adapt to changing conditions and better handle systems with multiple operating modes or discrete state changes. Therefore, switching sensors form a valuable tool in various applications, including aerospace, automotive control, nonlinear processes and robotics, where systems often switch between different operating regimes.

The design of soft sensors for single input and single output nonlinear systems was introduced and solved in [1], where a switching observer approach was developed. The approach is based on identifying linear approximants for different operating conditions of the original nonlinear model of the process and the development of a bank of linear observers. Also, it is based on the definition of observer-oriented target operating areas and the introduction of the dense web principle. Finally, a data-driven rule-based procedure was proposed to orchestrate the operation and the switching of the bank of observers. The performance of the approach was illustrated in [1] via its application to a nonlinear chemostat model.

In the present paper, following the set of assumptions in [1], the development of an extended soft sensor design approach that includes AI procedures is proposed. The inclusion of these procedures aims toward the improvement of the performance of soft sensors using switching observers. Two metaheuristic procedures were developed. The procedures were based on the linear approximants of the nonlinear dynamic SISO system and a set of linear full-order observers, which were computed using system identification data. Based on these two procedures, the switching procedure between observers in the bank of the observers was accomplished by increasing the width of the target operating areas. The cost criteria proposed in [1] were appropriately extended and modified in order to offer greater flexibility with respect to the selection of the observer parameters. It is important to mention that the switching observer design was complemented by a metaheuristic algorithm that was used for the specification of the observer parameters. The use of this algorithm facilitated the observer parameter selection, as well as selecting the width of the corresponding target operating areas. The development of the algorithm was imposed by the highly nonlinear and multi-cost minimization under the constraints goal of the problem at hand, where the analytic solution of the problem of determining the observer parameters did not seem to be possible.

The main results of the study are presented in Sections 3–8. In Section 2, the general framework for the design of soft sensors using switching observers is presented. The general form, as well as the basic assumptions of the structure of nonlinear SISO systems, is initially presented. Based on the general structure of the model, its linear approximant was computed, and a full-order state observer of a specific structure was designed. The observer matrices depended upon the identified model parameters of the linear approximant and the operating point of the process. In Section 3, new criteria for the determination of the observer parameters and the corresponding target operating areas are proposed. Due to the highly nonlinear nature of the newly proposed criteria, in Section 4, a metaheuristic algorithm of the type in [8,9] is proposed for both the determination of the necessary number of operating points and the evaluation of the observer parameters. The basic idea of the algorithm is to define an initial search area for the observer parameters and, after several loops, to converge to a suboptimal solution that satisfies the design goals. To validate the metaheuristic procedure, the problem of the development of soft sensors using switching observers for the case of an alcoholic fermentation process is investigated in Sections 5–8.

Industrial alcoholic fermentation processes are typical industrial processes with an essential impact on various industrial units, primarily for the production of ethanol (alcohol) and other valuable products. These processes rely on the metabolic activities of microorganisms, typically yeasts or bacteria, to convert sugars into alcohol and carbon dioxide. Alcoholic fermentation is a well-established and economically important process with applications in a range of industries and contributing to the production of fuel, beverages and various chemical products. Indicatively, see [10–12] for alcoholic fermentation technologies, [13–16] for alcoholic fermentation modeling, [17–19] for alcoholic fermentation optimization techniques and [20–22] for controller design.

Typically, in fermentation processes, not all system variables can be measured in real time. Also, the structure of the nonlinear dynamic model of the processes is available, but the physical parameters of the process are basically unknown to the designer. Consequently, the design of an observer/soft sensor scheme may be a critical component of process control and monitoring systems. See [23] for fault detection schemes, [24] for a bank-of-observer design, [25] for sliding mode observers, and [26–30] for other estimation and/or control aspects. The main advantages of the use of such soft sensing schemes lie in their cost-efficiency, non-invasiveness and flexibility, as well as the reduction in downtime that may be required compared with traditional sensors in the case of calibration or replacement. Specifically, for the alcoholic fermentation processes, the problem of fault detection and isolation using a combined parameter and state adaptive observer scheme was studied in [23]. A bank of local linear observers was designed for an alcoholic fermentation process in [24], where the design was based on the respective linear approximants of the mathematical description of the nonlinear process around operating points. A comparative analysis of the real-time performance of a family of sliding-mode observers for reconstructing key variables in a batch bioreactor for fermentative ethanol production was performed in [25]. The problem of estimation and control for alcoholic fermentation processes was investigated in [26] using adaptive controllers designed together with nonlinear estimation algorithms for unknown inputs and kinetics. The problem of designing online estimation strategies for imprecisely known kinetics of an alcoholic fermentation bioprocess was investigated in [27,28]. Toward this goal, an observer-based estimator, a regressive estimator and a high-gain observer were implemented. The behavior of the estimation scheme was investigated through computational experiments. The application of an observer scheme for state and parameter estimation of alcoholic processes was proposed in [29]. Finally, the problem of the simultaneous estimation of states and unknown inputs through high-gain nonlinear observers was investigated in [30] and the theoretical results were applied to an alcoholic fermentation process in a chemical semi-continuous fed-batch reactor.

With respect to the application of the present scheme to the alcoholic fermentation process, initially, the accuracy of the linear approximant of the process with respect to its nonlinear model was investigated. Second, the system property of I/O reconstructability of the state space linear approximant of the process was verified. Third, based on the linear approximant, a linear observer was designed for the estimation of the non-measurable variable of the process, where its parameters were derived through the identification of different operating points of the nonlinear model. Fourth, the operating points upon which identification was performed were determined using a metaheuristic algorithm so that the dense web principle was satisfied. The observers corresponding to the different operating points constituted a bank of observers. Fifth, the efficiency of the proposed scheme was verified through a series of computational experiments for both the switching observer scheme and the metaheuristic algorithm.

2. Preliminaries

In the present section, the general framework for the design of soft sensors using switching observers that was developed in [1] is presented. This framework is appropriately extended in the following sections. In the first subsection, the general form of nonlinear SISO systems and the basic assumptions/constraints on its form are presented. Then, based on the nonlinear model, the general form of its linear approximant is presented. Finally, based on the linear approximant, a full-order state observer is proposed, whose form depends not upon the true linear approximant parameters but upon identified linear approximant parameters.

2.1. A General Form of Nonlinear SISO Systems

A general form of nonlinear SISO dynamic systems is the following:

$$\frac{d\widetilde{x}(t)}{dt} = f_{NL}(\widetilde{x}, u);\ x(0-) = x_0,\ y(t) = c_{NL}(\widetilde{x}) \tag{1}$$

where $\widetilde{x}(t) \in \mathbb{R}^{n\times 1}$ denotes the state vector of the system, $y(t) \in \mathbb{R}$ denotes the vector of the measurable outputs of the system, $u(t) \in \mathbb{R}$ denotes the actuatable input of the system, $f_{NL}(\bullet,\bullet)$ $\left(: \mathbb{R}^{n+1} \to \mathbb{R}^n\right)$ is an $n \times 1$ nonlinear vector function and $c_{NL}(\bullet)$ $(: \mathbb{R}^n \to \mathbb{R})$ is a nonlinear function. Regarding the mathematical description in (1), the following considerations (see [1]) are assumed to hold:

i The nonlinear dynamic system (1) is globally stable.
ii The structure of $f_{NL}(\bullet,\bullet)$ is known. This structure depends on physical parameters.
iii The physical parameters in $f_{NL}(\bullet,\bullet)$ are in general not known to the designer. The parameters, being known, are those that are independent of the current operation conditions of the process.
iv The output and input variables of the process are measured in real time.
v The operating trajectory of the nonlinear process in an appropriate operation domain is known.

To present the operating trajectory, the nominal values of the state vector and the input and output variables are denoted as $\widetilde{X}$, U and Y, respectively. The operating trajectory is defined to be the set of all $\widetilde{X}$, U and Y so that $f_{NL}\left(\widetilde{X}, U\right) = 0$ and $Y = c_{NL}\left(\widetilde{X}\right)$. Following [1], the following is also assumed:

vi For every U, there exists a unique Y, i.e., $Y = h_{NL}(U)$, where $h_{NL}(\bullet)$ $(: \mathbb{R} \to \mathbb{R})$ is an appropriate function, which is known by the points $\ell = (Y, U)$ in $\mathbb{R}^2$, or a dense enough sample of them.

Under the above assumptions, the I/O operating trajectory of the nonlinear process is defined to be a graphical representation of the formula $Y = h_{NL}(U)$. The practical importance of the operating trajectory and the I/O operating trajectory is based on the stability of (1). According to the industrial practice (indicatively, see [3,4]), the system transitions are preserved around the I/O operational trajectory, where $\Delta\widetilde{x}(t) = \widetilde{x}(t) - \widetilde{X}$, $\Delta u(t) = u(t) - U$ and $\Delta y(t) = y(t) - Y$ are the variations of the system variables around the nominal values.

Mainly for presentation purposes and, secondarily, for analytic purposes, it was considered that the map of the vector of the state variables to the output variable was linear, i.e., $c_{NL}(\widetilde{x}) = c\widetilde{x}$ and the output matrix $c \in \mathbb{R}^{1\times n}$ is independent of the unknown physical parameters of the nonlinear system.

2.2. The Linear Approximant of the Nonlinear Dynamic System

The linear approximant of the dynamic system (1) is determined around $\widetilde{X}$, U and Y, corresponding to constant operating conditions for all system variables. The general form of the linear approximant of the model (1) is

$$\aleph : \begin{array}{l} \frac{d\Delta x_L(t)}{dt} = A\Delta x_L(t) + b\Delta u(t),\ \Delta y_L(t) = c\Delta x_L(t), \\ \Delta x_L(0-) = \Delta x_{L,0} = \widetilde{x}_0 - \widetilde{X}, \end{array} \tag{2}$$

where $\Delta y_L(t)$ and $\Delta x_L(t)$ aim to be the approximants of the deviations $\Delta y(t)$ and $\Delta\widetilde{x}(t)$, respectively, and where $\Delta u(t) = u(t) - U$. The response of the approximant is an accurate description of the nonlinear system response around the operating point $o(t) = \overline{o}$, where $o(t) = (u(t), \widetilde{x}(t), y(t))$ and $\overline{o} = (U, X, Y)$. The system matrices in (2) are evaluated using the formulas $A = \partial f_{NL}(\widetilde{x}, u)/\partial\widetilde{x}|_{o=\overline{o}}$ and $b = \partial f_{NL}(x, u)/\partial u|_{o=\overline{o}}$. Clearly, it holds that $A \in \mathbb{R}^{n\times n}$ and $b \in \mathbb{R}^{n\times 1}$.

Regarding the linear approximant, the following assumptions used in [1] are also considered to hold:

i The form of the linear approximant system matrices is known and depends upon independent physical parameters, which are considered to be unknown, as well as the nominal values of the system variables.
ii The linear approximant (2) is observable, independently of the nominal values of the system variables.
iii The state space linear approximant is asymptotically stable, independently of the nominal values of the system variables.
iv The nonlinear model of the process belongs to the class of systems with state space linear approximants that are I/O reconstructable using their respective I/O linear approximants.

For the definition of I/O reconstructability, see [1].

The I/O approximant of the system (2) is the following differential equation:

$$\mathfrak{S}: \Delta y_L^{(n_c)}(t) + h \begin{bmatrix} \Delta y_L^{(n_c-1)}(t) \\ \vdots \\ \Delta y_L^{(0)}(t) \\ -\Delta u^{(n_c-1)}(t) \\ \vdots \\ -\Delta u^{(0)}(t) \end{bmatrix} = 0, \quad (3)$$

where

$$h = \begin{bmatrix} h_D & | & h_N \end{bmatrix} = \begin{bmatrix} h_{D,1} & \dots & h_{D,n_c} & | & h_{N,1} & \dots & h_{N,n_c} \end{bmatrix} \in \mathbb{R}^{1\times 2n_c},$$

and where $h_{D,j}$ and $h_{N,j}$ ($j = 1, \dots, n_c$) are the real coefficients of the I/O approximant, with n_c being the rank of the controllability matrix of the linear approximant.

Defining $\mathbb{H}$ as the set of all admissible h and defining $\mathbb{H}_L$ as the set of all admissible ℓ, under assumption (vi) in Section 2.1, the system matrices of (2) can be expressed as functions of ℓ (or equivalently of U) and h, i.e.,

$$A = A(h, U) \in \mathbb{R}^{n\times n},\ b = b(h, U) \in \mathbb{R}^{n\times 1},\ c = c(h, U) \in \mathbb{R}^{1\times n}. \quad (4)$$

In practice, the I/O approximant can be determined through data-driven approaches, like the identification of the coefficients of the I/O approximant in (3), using measurements of the input and output of the system. The I/O linear approximant dynamic system relating the variations of the outputs to the variations of the inputs is of the following form:

$$\mathfrak{S}_I: \Delta y^{(n_c)}(t) + \hat{h} \begin{bmatrix} \Delta y^{(n_c-1)}(t) \\ \vdots \\ \Delta y^{(0)}(t) \\ -\Delta u^{(n_c-1)}(t) \\ \vdots \\ -\Delta u^{(0)}(t) \end{bmatrix} + \varepsilon_I(t) = 0, \quad (5)$$

where

$$\hat{h} = \begin{bmatrix} \hat{h}_D & | & \hat{h}_N \end{bmatrix} = \begin{bmatrix} \hat{h}_{D,1} & \dots & \hat{h}_{D,n_c} & | & \hat{h}_{N,1} & \dots & \hat{h}_{N,n_c} \end{bmatrix} \in \mathbb{R}^{1\times 2n_c}, \quad (6)$$

$\hat{h}_{D,j}$ and $\hat{h}_{N,j}$ are the identified parameters, and $\varepsilon_I(t)$ is the modeling error resulting from the identification. The present type of identification can be accomplished through several methods; indicatively, see the methods in [31–37].

The linear approximant system matrices corresponding to the above parameter estimation are expressed using the following formulae:

$$A = A\left(\hat{h}, U\right) \in \mathbb{R}^{n\times n},\ b = b\left(\hat{h}, U\right) \in \mathbb{R}^{n\times 1},\ c = c\left(\hat{h}, U\right) \in \mathbb{R}^{1\times n}. \quad (7)$$

For the above system matrix, it is required to remain stable.

2.3. The Proposed Full-Order State Observer Design

A full-order observer, which depends on the identified parameters of the I/O linear approximant system where $\hat{h}$, U and Y are known, was proposed in [1]. The observer is

$$\Im : \Delta\dot{z}(t) = F\left(\hat{h}, U\right)\Delta z(t) + g\left(\hat{h}, U\right)\Delta y(t) + m\left(\hat{h}, U\right)\Delta u(t),\ \ \Delta z(0-) = \Delta z_0, \tag{8}$$

where Δz is the estimation of $\Delta\widetilde{x}$, and $F\left(\hat{h}, U\right) \in \mathbb{R}^{n\times n}$, $m\left(\hat{h}, U\right) \in \mathbb{R}^{n\times 1}$ and $g(\hat{h}, U) \in \mathbb{R}^{1\times n}$ are appropriate observer matrices to be selected by the designer. The matrices F and m are

$$F\left(\hat{h}, U\right) = A\left(\hat{h}, U\right) - g\left(\hat{h}, U\right)c\left(\hat{h}, U\right). \tag{9}$$

$$m\left(\hat{h}, U\right) = b\left(\hat{h}, U\right). \tag{10}$$

The elements of $g\left(\hat{h}, U\right)$ are selected such that the eigenvalues of $F\left(\hat{h}, U\right)$ are appropriately adjusted. Let $C_a^- = \{s \in C : \mathrm{Re}\{s\} < -a\}$, where $a \geq 0$. Here, the design goal is for the eigenvalues of $F\left(\hat{h}, U\right)$ to a-regional stable, real and distinct, i.e., they belong in C_a^- and are ordered as follows:

$$0 \leq a < \rho_{F,1}\left(\hat{h}, U\right) < \cdots < \rho_{F,n}\left(\hat{h}, U\right). \tag{11}$$

Similarly to [1], the linear approximant derived after substituting the parameters of the I/O approximant using the respective identified parameters and involving the variations of the real variables of the nonlinear system is expressed as follows:

$$\Delta\dot{\widetilde{x}}(t) = A\left(\hat{h}, U\right)\Delta\widetilde{x}(t) + b\left(\hat{h}, U\right)\Delta u(t) + \varepsilon_x(t),\ \ \Delta\widetilde{x}(0-) = \widetilde{x}(0-) - \widetilde{X}. \tag{12}$$

where $\varepsilon_x(t)$ is the modeling error between the nonlinear model (1) and the above linear approximant. From (8) and (12), the observer estimation error is

$$\dot{e}_O(t) = F\left(\hat{h}, U\right)e_O(t) + \varepsilon_x(t),\ \ e_O(0-) = e_{O,0}. \tag{13}$$

The solution of the above system of differential equations is

$$e_O(t) = e_{O,A}(t) + e_{O,B}(t), \tag{14}$$

where

$$\dot{e}_{O,A}(t) = F\left(\hat{h}, U\right)e_{O,A}(t),\ \ e_{O,A}(0-) = e_{O,0}, \tag{15}$$

$$\dot{e}_{O,B}(t) = F\left(\hat{h}, U\right)e_{O,B}(t) + \varepsilon_x(t),\ \ e_{O,B}(0-) = 0_{n\times 1}. \tag{16}$$

In order to express the solution of (15) and since the eigenvalues of $F\left(\hat{h}, U\right)$ are constrained to be a-regional stable, it can be verified that (see also [1])

$$e_{O,A}(t) = \left[\sum_{k=1}^{n} \exp\left(-\rho_{F,k}\left(\hat{h}, U\right)t\right)\Phi_k\left(\hat{h}, U\right)\right]e_{O,0};\ k = 1, \ldots, n, \tag{17}$$

where

$$\Phi_k\left(\hat{h}, U\right) = \lim_{s\to\rho_{F,k}(\hat{h},U)}\left[\left(s + \rho_{F,k}\left(\hat{h}, U\right)\right)\left(sI_n - F\left(\hat{h}, U\right)\right)^{-1}\right]. \tag{18}$$

In order to express the steady-state values of the solution of (16), similarly to [1], the case of stepwise responses will be considered, i.e., the input of the system will be considered to be of the step form

$$u(t) = U + u_w u_s(t). \tag{19}$$

where $u_s(t)$ is the unit step signal and u_w is a positive real number, denoting the amplitude of the input. From (12), it can be verified that the steady-state value of the modeling error is of the form

$$\varepsilon_{x,SS}\left(\hat{h}, U, u_w\right) = \lim_{t\to+\infty} \varepsilon_x(t) = -A\left(\hat{h}, U\right)\left(\widetilde{X}_w - \widetilde{X}\right) - b\left(\hat{h}, U\right)u_w, \tag{20}$$

where $\widetilde{X}_w$ is the vector of the steady-state values of the state variables after the application of the step input signal. From (16) and (20), it can be verified that the vector of the steady-state values of the elements of the estimation error is of the form

$$e_{O,SS}\left(\hat{h}, U, u_w\right) = \left(A(\hat{h}, U) - g\left(\hat{h}, U\right)c\right)^{-1} \varepsilon_{x,SS}\left(\hat{h}, U, u_w\right). \tag{21}$$

The above analysis is used in the following section to produce a new type of criterion for the determination of the observer parameters.

3. A New Criteria for the Determination of the Observer Parameters

In the present section, based on the results presented in Section 2, new criteria for the determination of the observer parameters and the corresponding target operating areas are proposed. In particular, the design criteria are based on the transient response of the observer, as well as the resulting steady-state error. With respect to the transient response part, the approach presented in [1] is used. With respect to the steady state error, a multimetric scheme, which appears to offer increased flexibility on the resulting observer performance, is proposed. The present section concludes with the presentation of an observer-switching scheme between different operating points.

3.1. Design Requirements

From (17) and (18), it can be observed that

$$\|e_{O,A}(t)\|_\alpha < \exp(-at)\left[\sum_{k=1}^{n}\left\|\Phi_k\left(\hat{h}, U\right)\right\|_\alpha\right]\|e_{O,0}\|_\alpha,\ \forall t \geq 0. \tag{22}$$

To guarantee that $\|e_{O,A}(t)\|_\alpha$ is enough small for all initial conditions, it is required that the following cost function (see also [1]) is enough small, i.e.,

$$J^*_{e,A}\left(\hat{h}, U, \rho_F\right) = \exp(-a)\left[\sum_{k=1}^{n}\left\|\Phi_k\left(\hat{h}, U\right)\right\|_\alpha\right] \leq \zeta_e, \tag{23}$$

where $\zeta_e \in \mathbb{R}_+$ is a positive real number set by the designer.

Regarding the steady-state error, an extension of the design goal in [1] is proposed. Here, a set of cost criteria, where each criterion refers to only one state variable, is proposed. In particular, the ratio of the steady-state estimation error to the steady state of the variation of the state vector is required to be appropriately bounded. These cost criteria requirements are the following:

$$\left(J^*_{e,O}\right)_j\left(\hat{h}, U, \rho_F, u_w\right) = \left|\frac{\left(e_{O,SS}\right)_j\left(\hat{h}, U, u_w\right)}{\left(\widetilde{X}_w\right)_j - \widetilde{X}_j}\right| \leq \zeta_{SS,j};\ \forall j \in \{1, \ldots, n\}, \tag{24}$$

where $\left(\widetilde{X}_w\right)_j$, $\widetilde{X}_j$ and $\left(e_{O,SS}\right)_j\left(\hat{h}, U, u_w\right)$ are the jth elements of $\widetilde{X}_w$, $\widetilde{X}$ and $e_{O,SS}\left(\hat{h}, U, u_w\right)$, respectively, and $\left(\zeta_{SS}\right)_j$ are small enough positive real numbers set by the designer. It is important to mention that the inequality constraint in (24) is different than that proposed in [1], as the constraint in [1] is an overall Euclidean norm type of steady-state error metric. The herein-proposed multimetric scheme more accurately represents the different physical characteristics of each state variable and offers increased flexibility on the resulting observer performance.

The observer design procedure is completed by determining the elements of ρ_F so that $|u_w|$ is maximized under the constraints in (23) and (24). Clearly, this is a quite complex nonlinear maximization problem under constraints. Its analytic solution is hard to determine. Toward solving this maximization problem under inequality constraints, a metaheuristic algorithm of the type in [8,9] is proposed in Section 4. The goal of the algorithm is the numerical determination of ρ_F, resulting in a suboptimal solution satisfying the inequality constraints.

In the following subsection, the consequences of the herein-proposed multimetric criterion to the switching scheme are presented.

3.2. Switching Scheme

According to [1] and the above analysis, the observer matrices depend upon the operating point of the system belonging to a prespecified set of operating points of the systems denoted as $L = \{\ell_1, \ell_2, \ldots, \ell_\mu\}$, where $\ell_i = (Y_i, U_i)$ and where Y_i and U_i denote the respective nominal output and input values of ℓ_i, where $i \in \{1, \ldots, \mu\}$. This set is called the set of nominal operating points. Around each nominal operating point ℓ_i, the nonlinear system is approximated using a respective linear state space approximant denoted as $\aleph_i = (A_i, b_i, c_i)$ and evaluated using (7), where $\hat{h}_i$ are the respective identified I/O linear approximant coefficients. Thus, for each nominal operating point, the respective observer matrices are of the form $F\left(\hat{h}_i, U_i\right)$, $g\left(\hat{h}_i, U_i\right)$ and $m\left(\hat{h}_i, U_i\right)$. For each nominal operating point set, the corresponding set of observer parameters is denoted by ${}^i\rho_F\left(\hat{h}_i, U_i\right)$. Clearly, a bank of observers, with one per operating point, is designed. The bank of observers includes the observers $\Im_1, \ldots, \Im_\mu$ and is coordinated using a switching mechanism that appropriately enables the operation of appropriately chosen observers of the bank.

The presentation of the cost function introduced in the previous subsection is completed by presenting its influence on the determination of the target operating areas. To this end, the primary module of the stepwise safe transition, namely, the transition from an initial operating point, denoted by $\ell_I = (Y_I, U_I)$, to a destination operating point, denoted by $\ell_D = (Y_D, U_D)$, is necessary. The nominal value of the state vector at the initial operating point is denoted by $\widetilde{X}_I$ and the nominal value of the state vector at the destination operating point is denoted by $\widetilde{X}_D$. The observer used during this transition is determined by the nominal operating point $\ell_i = (Y_i, U_i)$ and the respective identified data $\hat{h}_i$. For the observer to be applied to the nonlinear system, the nominal value of the state vector, denoted by $\widetilde{X}_i$ and corresponding to $\ell_i = (Y_i, U_i)$, is added to the estimated state vector produced by the linear observer. Following [1] and using (23) and (24), the target operating area of each operating point is determined in terms of the new cost function as follows:

$$\begin{gathered}\mathbb{T}(U_i) = [U_i - u_{i,\max}, U_i + u_{i,\max}] \subseteq {}^i\mathbb{T}_O\left(\hat{h}_i, U_i, {}^i\zeta_e, {}^i\zeta_{SS,j}\right), \\ u_{i,\max} = \max\left\{u_i \in \mathbb{R}_+ : [U_i - u_i, U_i + u_i] \subseteq {}^i\mathbb{T}_O\left(\hat{h}_i, U_i, {}^i\zeta_e, {}^i\zeta_{SS,j}\right)\right\},\end{gathered} \tag{25}$$

where

$$\begin{gathered}{}^i\mathbb{T}_O(\hat{h}_i, U_i, a, \chi_{O,A}, \chi_{O,B}) = \left\{(U_I, U_D) \in \mathbb{R} \times \mathbb{R} : \left({}^iJ^*_{e,A}\left(\hat{h}_i, U_i, {}^i\rho_F\right) \leq {}^i\zeta_e\right) \wedge \right. \\ \left. \left({}^i\left(J^*_{e,O}\right)_j\left(\hat{h}_i, U_i, a_i, U_D - U_i\right) \leq {}^i\zeta_{SS,j}, \forall j \in \{1, \ldots, n\}\right); u(t) = (U_D - U_i)u_s(t) + U_I\right\}.\end{gathered} \tag{26}$$

According to [1] and assuming that

$$\text{if } \mu > 1 \text{ and } U_i < U_{i+1},\ \forall i \in \{1, \dots, \mu - 1\}, \tag{27}$$

then the dense web principle is expressed as

$$\mathbb{T}(U_i) \cap \mathbb{T}(U_{i+1}) \neq \varnothing,\ \forall i \in \{1, \dots, \mu - 1\}. \tag{28}$$

The stepwise transitions are safe if the transition from one initial operating point $\ell_I = (Y_I, U_I)$ to a destination operating point $\ell_D = (Y_D, U_D)$, where $U_I \leq U_D$ is divided to create appropriate individual transitions. To define these transitions, let $U_I \in \mathbb{T}(U_i)$ and $U_D \in \mathbb{T}(U_{i+\nu})$, where $i \in \{1, \dots, \mu\}$ and $\nu \in \{0, \dots, \mu - i\}$. Let

$$\nu_\sigma = \max\{k \in \{i + \sigma - 1, \dots, \nu\} : \mathbb{T}(U_{i+\nu_{\sigma-1}}) \cap \mathbb{T}(U_k) \neq \varnothing\},\ \sigma \in \{0, \dots, \nu\}. \tag{29}$$

The first transition is from $\ell_I = (Y_I, U_I)$ to the intermediate destination point $\ell_{D,1} = (Y_{D,1}, U_{D,1})$, where $U_{D,1} \in \mathbb{T}(U_i) \cap \mathbb{T}(U_{i+\nu_1})$. The second transition is from $\ell_{D,1} = (Y_{D,1}, U_{D,1})$ to $\ell_{D,2} = (Y_{D,2}, U_{D,2})$, where $U_{D,2} \in \mathbb{T}(U_{i+\nu_1}) \cap \mathbb{T}(U_{i+\nu_2})$. The transitions continue till the final destination point, denoted as $\ell_{D,f} = \left(Y_{D,f}, U_{D,f}\right)$, where $U_{D,f} \in \mathbb{T}\left(U_{i+\nu_{f-1}}\right) \cap \mathbb{T}\left(U_{i+\nu_f}\right)$ and $\nu_f = \nu$. $\ell_{D,f} = \ell_D = (Y_D, U_D)$ and f is the total number of the transitions. The transition from $\ell_D = (Y_D, U_D)$ to $\ell_I = (Y_I, U_I)$ is the reverse sequence of steps.

Due to the highly nonlinear nature of the inequalities in (23) and (24), as well as the definition of the target operating areas, the analytic determination of the observer parameters and the target operating areas is a daunting task. In order to derive a solution to this problem despite its complexity, a metaheuristic algorithm is proposed in the next section.

4. A Metaheuristic Algorithm toward Determination of the Target Operating Areas

In the present section, taking advantage of the property that the unknown quantities are real numbers, a metaheuristic algorithm of the type in [8,9] is proposed for both the determination of the necessary number of operating points and the evaluation of the observer parameters. The basic idea of the algorithm is to compute a suboptimal solution that satisfies the design goals upon first defining an initial search area for the observer parameters ρ_F. After the execution of several loops, the algorithm converges to the suboptimal solution. For the execution of the algorithm, an appropriate cost function that is minimized by the algorithm under all necessary constraints is defined.

Let U_i $(i = 1, \dots, \mu)$ be the nominal value of the input around which the target operating area must be determined and $\hat{h}_i$ be the identified I/O parameters of the linear approximant of the system corresponding to U_i. In what follows, it is assumed that U_i and $\hat{h}_i$ were previously determined. Let ${}^i\rho_F$ be the corresponding observer parameters and ${}^iu_w$ be the half-width of the target operating area. Here, the performance criterion to be minimized is selected to be of the form

$$Q\left(\hat{h}_i, U_i, {}^i\rho_F, {}^iu_w\right) = \gamma_{e,A} J^*_{e,A}\left(\hat{h}_i, U_i, {}^i\rho_F\right)^2 + \sum_{j=1}^{n} (\gamma_{e,O})_j (J^*_{e,O})_j \left(\hat{h}_i, U_i, {}^i\rho_F, {}^iu_w\right)^2 + \sum_{j=1}^{n} (\gamma_F)_j \rho_{F,j}\left(\hat{h}_i, U_i\right)^2 + \gamma_w \left({}^iu_w\right)^{-2} \tag{30}$$

where $\gamma_{e,A}$, $(\gamma_{e,O})_j$, $(\gamma_F)_j$ and γ_w $(j = 1, \dots, n)$ are non-negative real weight factors constrained to satisfy the equality

$$\gamma_{e,A} + \sum_{j=1}^{n} (\gamma_{e,O})_j + \sum_{j=1}^{n} (\gamma_F)_j + \gamma_w = 1. \tag{31}$$

Clearly, the weight factors can be used to adjust the influence/importance of each term to the performance criterion. Furthermore, considering that the performance criterion in (30) incorporates quantities of different natures that are expressed in different units and of different orders of magnitude, the weight factors serve as the normalization coefficients of the various quantities. Note that the positive exponent in the first three terms implies improved performance for smaller values of the respective metrics, while the negative exponent in the last term leads to improved performance for larger values of ${}^{i}u_w$, corresponding to a larger operating area. Minimization of the performance criterion in (30) and (31) must be made under the constraints in (11), (23) and (24) by appropriately selecting ${}^{i}\rho_F$ and ${}^{i}u_w$. Let n_{loop}, n_{rep} and n_{total} be the number of loops, the number of loop repetitions and the total allowable number of computations, respectively. Also, let $\sigma \in \mathbb{R}_+$ be a convergence metric of the search algorithm, and $(\widetilde{\rho}_{F,j})\left(\hat{h}_i, U_i\right)$, $\left(\widehat{\rho}_{F,j}\right)\left(\hat{h}_i, U_i\right)$, ${}^{i}\widetilde{u}_w$ and ${}^{i}\widehat{u}_w$ be the bounds of the observer parameters, defining a search area for each parameter being of the form

$$(\widetilde{\rho}_{F,j})\left(\hat{h}_i, U_i\right) \leq \rho_{F,j}\left(\hat{h}_i, U_i\right) \leq \left(\widehat{\rho}_{F,j}\right)\left(\hat{h}_i, U_i\right) \tag{32}$$

$${}^{i}\widetilde{u}_w \leq {}^{i}u_w \leq {}^{i}\widehat{u}_w \tag{33}$$

From the bounds in (32) and (33), the respective half-widths and the center value can be evaluated using

$$\left(\rho_{F,j}\right)_w\left(\hat{h}_i, U_i\right) = \left(\widehat{\rho}_{F,j}\right)\left(\hat{h}_i, U_i\right) - (\widetilde{\rho}_{F,j})\left(\hat{h}_i, U_i\right) \tag{34}$$

$$\left(\rho_{F,j}\right)_c\left(\hat{h}_i, U_i\right) = \left[\left(\widehat{\rho}_{F,j}\right)\left(\hat{h}_i, U_i\right) + (\widetilde{\rho}_{F,j})\left(\hat{h}_i, U_i\right)\right]/2 \tag{35}$$

$$\left({}^{i}u_w\right)_w = {}^{i}\widehat{u}_w - {}^{i}\widetilde{u}_w \tag{36}$$

$$\left({}^{i}u_w\right)_c = \left({}^{i}\widehat{u}_w + {}^{i}\widetilde{u}_w\right)/2 \tag{37}$$

In each cycle of the metaheuristic algorithm, a superset of n_{loop} sets of observer parameters is determined that satisfy the constraints in (11), (23) and (24). For each set of observer parameters belonging to the superset, the cost criterion in (30) and (31) is evaluated and the optimal value is extracted. This procedure is repeated for a total number of n_{rep}, producing a new superset containing the n_{rep} optimal observer parameters, which are determined in each repetition. From the second superset, the optimal set of observer parameters defines the new center values of observer parameters. The updated half-widths are evaluated as the difference between the maximum and minimum values of each parameter in the second superset. The above procedure is repeated until all observer parameters converge to a certain value, i.e., when

$$\left|\frac{\left(\rho_{F,j}\right)_w\left(\hat{h}_i, U_i\right)}{\left(\rho_{F,j}\right)_c\left(\hat{h}_i, U_i\right)}\right| < \sigma \;\; \forall j \in \{1, \ldots, n\} \text{ and } \left|\frac{\left({}^{i}u_w\right)_w}{\left({}^{i}u_w\right)_c}\right| < \sigma \tag{38}$$

The algorithm aborts unsuccessfully if a total number of n_{total} sets of observer parameters are generated.

The analytic form of the metaheuristic algorithm is given as Algorithm 1.

Algorithm 1 Metaheuristic Algorithm

Inputs

- The nominal value U_i and the respective identified model parameters $\hat{h}_i$.
- The performance criterion $Q\left(\hat{h}_i, U_i, {}^i\rho_F, {}^iu_w\right)$.
- The bounds ζ_e and $\zeta_{SS,j}$ $(j = 1, \ldots, n)$.
- Center values and half-widths for the initial search area of the parameters $\left(\rho_{F,j}\right)_w\left(\hat{h}_i, U_i\right)$ and $\left(\rho_{F,j}\right)_c\left(\hat{h}_i, U_i\right)$ $(j = 1, \ldots, n)$, as well as $\left({}^iu_w\right)_w$ and $\left({}^iu_w\right)_c$.
- The stability margin a_i.
- The iteration parameters $n_{loop}, n_{rep}, n_{total} \in \mathbb{N}$.
- The convergence threshold σ.

Outputs

- The observer poles $\rho_{F,j}\left(\hat{h}_i, U_i\right)$ $(j = 1, \ldots, n)$.

Algorithm

1: Set the numbering index $i_{\max} = 0$.
2: Determine a search area $\Im$ for the observer parameters according to the inequalities in (27).
3: **for** $i_1 = 1, \ldots, n_{rep}$.
4: **for** $i_2 = 1, \ldots, n_{loop}$
5: Set the numbering index $i_{\max} = i_{\max} + 1$.
6: **if** $i_{\max} > n_{total}$
7: Go to 22.
8: **end if**
9: Randomly select a set of observer parameters within the search area $\Im$, let $\rho_{F,j}\left(\hat{h}_i, U_i\right) = \left(\rho_{F,j}\right)_{i_2}\left(\hat{h}_i, U_i\right)$ $(j = 1, \ldots, n)$ and ${}^iu_w = \left({}^iu_w\right)_{i_2}$.
10: **if** the conditions in (11), (23) and (24) are not satisfied
11: Go to 9.
12: **end if**
13: Evaluate $Q_{i_2} = Q\left(\hat{h}_i, U_i, \left({}^i\rho_F\right)_{i_2}, \left({}^iu_w\right)_{i_2}\right)$.
14: **end for**
15: Find $Q_{i_1,\min} = \min\left\{Q_{i_2}, i_2 = 1, \ldots, n_{loop}\right\}$, as well as the corresponding observer parameters; let $\left(\rho_{F,j}\right)_{i_1}\left(\hat{h}_i, U_i\right)$ $(j = 1, \ldots, n)$ and $\left({}^iu_w\right)_{i_1}$.
16: **end for**
17: Find the parameters $\left(\rho_{F,j}\right)_{\min}\left(\hat{h}_i, U_i\right)$ and $\left({}^iu_w\right)_{\min}$ corresponding to $Q_{\min} = \min\{Q_{i_1,\min}, i_1 = 1, \ldots, n_{rep}\}$, as well as the ranges $\delta\rho_{F,j}\left(\hat{h}_i, U_i\right) = \max\left\{\left(\rho_{F,j}\right)_{i_1}\left(\hat{h}_i, U_i\right), i_1 = 1, \ldots, n_{rep}\right\} - \min\left\{\left(\rho_{F,j}\right)_{i_1}\left(\hat{h}_i, U_i\right), i_1 = 1, \ldots, n_{rep}\right\}$ $(j = 1, \ldots, n)$ and ${}^i\delta u_w = \max\left\{\left({}^iu_w\right)_{i_1}, i_1 = 1, \ldots, n_{rep}\right\} - \min\left\{\left({}^iu_w\right)_{i_1}, i_1 = 1, \ldots, n_{rep}\right\}$.
18: Define

$$\left(\rho_{F,j}\right)_c\left(\hat{h}_i, U_i\right) = \left(\rho_{F,j}\right)_{\min}\left(\hat{h}_i, U_i\right) \; (j = 1, \ldots, n),$$
$$\left(\widetilde{\rho}_{F,j}\right)\left(\hat{h}_i, U_i\right) = \left(\rho_{F,j}\right)_c\left(\hat{h}_i, U_i\right) - \delta\rho_{F,j}\left(\hat{h}_i, U_i\right) \; (j = 1, \ldots, n),$$
$$\left(\widehat{\rho}_{F,j}\right)\left(\hat{h}_i, U_i\right) = \left(\rho_{F,j}\right)_c\left(\hat{h}_i, U_i\right) + \delta\rho_{F,j}\left(\hat{h}_i, U_i\right) \; (j = 1, \ldots, n),$$
$$\left({}^iu_w\right)_c = \left({}^iu_w\right)_{\min}, \; {}^i\widetilde{u}_w = \left({}^iu_w\right)_c - {}^i\delta u_w, \; {}^i\widehat{u}_w = \left({}^iu_w\right)_c + {}^i\delta u_w,$$

and evaluate $\left(\rho_{F,j}\right)_w\left(\hat{h}_i, U_i\right)$ $(j = 1, \ldots, n)$ and $\left({}^iu_w\right)_w$ using (34) and (36).
19: **if** the inequalities in (38) are not satisfied
20: Go to 2.
21: **end if**
22: Set $\rho_{F,j}\left(\hat{h}_i, U_i\right) = \left(\rho_{F,j}\right)_{\min}\left(\hat{h}_i, U_i\right)$ $(j = 1, \ldots, n)$ and ${}^iu_w = \left({}^iu_w\right)_{\min}$.

It is important to mention that the above algorithm determines the target area for a given nominal value of the input. Clearly, this procedure must be repeated for a large enough number of points so that a desired area is covered through target operating areas satisfying the dense web principle. Let $U^*_{\min}$ and $U^*_{\max}$ be the minimum and maximum values of the area that needs to be covered through target operating areas satisfying the dense web principle. Furthermore, let n_p be an initial number of points of nominal values of the input to be selected within $U^*_{\min}$ and $U^*_{\max}$, i.e., $U^*_{\min} < U_i < U^*_{\max}$ for $i = 1, \ldots, n_p$. In what follows, it is assumed that these points are uniformly distributed and, without loss of generality, that $U^*_{\min} < U_1 < U_2 < \ldots < U_{n_p} < U^*_{\max}$. Toward determination of the total number of points needed to cover all the area between $U^*_{\min}$ and $U^*_{\max}$, the following Algorithm 2 is proposed.

Algorithm 2 Determination of the number of input nominal value points

Inputs

- The minimum and maximum values $U^*_{\min}$ and $U^*_{\max}$.
- The initial number of points n_p.

Outputs

- The set of target operating areas

Algorithm

1: Create a uniform grid of n_p nominal values of the input so that $U^*_{\min} < U_i < U^*_{\max}$ $(i = 1, \ldots, n_p)$.
2: **for** $i = 1, \ldots, n_p$
3: Identify the unknown I/O system parameters $\hat{h}_i$.
4: Evaluate the target operating areas corresponding to the nominal value of the input.
5: **end for**
6: Examine whether the dense web principle is satisfied.
7: **if** the dense web principle is satisfied
8: Go to 15.
9: **else**
10: Find the areas that remain uncovered and select additional points in the middle of the uncovered areas.
11: Identify the unknown I/O system parameters for the additional points.
12: Evaluate the target operating areas of each additional point
13: **end if**
14: Go to 6.
15: Eliminate the superfluous points corresponding to target areas covered by other ones.

The two algorithms constitute a unified approach toward determining both the target operating areas satisfying the dense web principle and the observer parameters corresponding to these areas.

5. Applications to Alcoholic Fermentation Dynamics

In Sections 5 and 6, the theoretical tools presented in Sections 2–4 are shown to be validated through the application of the tools to the mathematical model of an alcoholic fermentation process. In the present section, after presenting the nonlinear model of the process, the respective linear approximant is derived. The accuracy of the linear approximant compared with the original nonlinear model is examined through a series of computational experiments.

5.1. Nonlinear System Model

The dynamics of the process are described using a nonlinear system of equations of the form (1) (see [23,24]), where

$$\tilde{x}(t) = \begin{bmatrix} \tilde{x}_1(t) & \tilde{x}_2(t) \end{bmatrix}^T = \begin{bmatrix} C(t) & S(t) \end{bmatrix}^T, \; f_{NL}(\tilde{x}, u) = \begin{bmatrix} (f_{NL})_1(\tilde{x}, u) & (f_{NL})_2(\tilde{x}, u) \end{bmatrix}^T, \quad (39)$$

$$(f_{NL})_1(\widetilde{x},u) = (\mu(t) - u(t))\widetilde{x}_1(t),\ (f_{NL})_2(\widetilde{x},u) = -\frac{1}{Y_{c/s}}\mu(t)\widetilde{x}_1(t) + (S_a - \widetilde{x}_2(t))u(t), \tag{40}$$

$$\mu_b(t) = \mu_m\widetilde{x}_2(t)/(K_s + \widetilde{x}_2(t)),\ c_{NL}(\widetilde{x}) = \widetilde{x}_2 \tag{41}$$

and where C and S are the biomass and substrate concentrations in the bioreactor, respectively; u is the dilution rate (actuatable input); S_a is the influent substrate concentration; μ_b is biomass growth rate; μ_m is the maximum growth rate; K_s is the saturation constant; and $Y_{c/s}$ is the yield coefficient. Note that the influent substrate concentration is considered herein to be constant. From the form of $c_{NL}(\widetilde{x})$, it can readily be observed that the output of the system can be rewritten in the form $y(t) = cx(t)$, where $c = \begin{bmatrix} 0 & 1 \end{bmatrix}$. Finally, let $x(0-) = x_0$ be the initial conditions of the nonlinear model (39)–(41).

5.2. Linear Approximant

From (39)–(41), it can be proved that there exist two types of operating points. These two types of operating points are

$$\widetilde{X} = \begin{bmatrix} \widetilde{X}_1 \\ \widetilde{X}_2 \end{bmatrix} = \begin{bmatrix} Y_{c/s}(S_a - K_s/(\mu_m U^{-1} - 1)) \\ K_s/(\mu_m U^{-1} - 1) \end{bmatrix}, \tag{42}$$

$$\widetilde{X} = \begin{bmatrix} \widetilde{X}_1 \\ \widetilde{X}_2 \end{bmatrix} = \begin{bmatrix} 0 \\ S_a \end{bmatrix}. \tag{43}$$

Clearly, the second type of operating points corresponds to the washout conditions (see [38,39]), which is undesirable. By applying a series of computations and considering that the dilution rate is positive, as is expected, it can be proven that (31a) is a stable operating point if and only if

$$U \in (0, U_{\max}), \tag{44}$$

where $U_{\max} = S_a\mu_m/(K_s + S_a)$. If $U \in [U_{\max}, +\infty)$, then the only feasible operating point is (43). Hence, in order to guarantee normal operating conditions, the nominal value of the state vector will be considered to satisfy (42). Using (44), the ranges of the nominal values of the state variables are computed to be

$$\widetilde{X}_1 \in \left(\widetilde{X}_{1,\min}, \widetilde{X}_{1,\max}\right);\ \widetilde{X}_{1,\min} = 0,\ \widetilde{X}_{1,\max} = S_a Y_{c/s}, \tag{45}$$

$$\widetilde{X}_2 \in \left(\widetilde{X}_{2,\min}, \widetilde{X}_{2,\max}\right);\ \widetilde{X}_{2,\min} = 0,\ \widetilde{X}_{2,\max} = S_a. \tag{46}$$

Using (42), the linear approximant of the process around $\widetilde{X}$ in (42) is computed to be of the form (2), where

$$A = \begin{bmatrix} 0 & \frac{Y_{c/s}(U-\mu_m)[(K_s+S_a)U - S_a\mu_m]}{K_s\mu_m} \\ -\frac{U}{Y_{c/s}} & -\frac{K_sU^2 + S_a(U-\mu_m)^2}{K_s\mu_m} \end{bmatrix},\ b = \begin{bmatrix} Y_{c/s}\left(\frac{K_sU}{\mu_m - U} - S_a\right) \\ S_a - \frac{K_sU}{\mu_m - U} \end{bmatrix}. \tag{47}$$

From (47) it can be verified that the characteristic polynomial of $\aleph_L$ is of the form

$$p(s) = s^2 + s\frac{K_sU^2 + S_a(U-\mu_m)^2}{K_s\mu_m} + \frac{U(U-\mu_m)[(K_s+S_a)U - S_a\mu_m]}{K_s\mu_m}, \tag{48}$$

while its roots are computed to be

$$r_1 = -U,\ r_2 = -\frac{(U-\mu_m)[(K_s+S_a)U - S_a\mu_m]}{K_s\mu_m}. \tag{49}$$

Applying elementary manipulations, the I/O description of the linear approximant of the process takes on the form

$$\mathfrak{S} : \Delta_L \dot{y}(t) + h_D \Delta_L y(t) = h_N \Delta u(t), \tag{50}$$

where

$$h_D = -r_2,\ h_N = S_a + K_s U/(U - \mu_m). \tag{51}$$

Clearly, the transfer function is $H(s) = h_N/(s + h_D)$. Note that by using the definitions in (51), the linear approximant system matrices in (47) can be rewritten as

$$A = \begin{bmatrix} 0 & Y_{c/s} h_D \\ -U/Y_{c/s} & -(h_D + U) \end{bmatrix},\ b = \begin{bmatrix} -Y_{c/s} h_N \\ h_N \end{bmatrix}. \tag{52}$$

5.3. Accuracy of the Linear Approximant

The accuracy of the response (forced response plus free response) of the linear approximant compared with the respective response of the nonlinear process is investigated through the following norm-type cost functions (see also [1,2]):

$$J_\infty = \frac{\max\limits_{j=1,2} \left\{ \sup\limits_{t \in [t_0, (T_{\max})_j]} \left| \widetilde{x}_j(t) - \Delta_L \widetilde{x}_j(t) - \widetilde{X}_j \right| \right\}}{\max\limits_{j=1,2} \left\{ \sup\limits_{t \in [t_0, (T_{\max})_j]} \left| \Delta_L \widetilde{x}_j(t) \right| \right\}} \times 100\%, \tag{53}$$

$$J_1 = \left(\frac{\sum\limits_{j=1}^{2} \left[\lim\limits_{t \to +\infty} \left| \widetilde{x}_j(t) - \Delta_L \widetilde{x}_j(t) - \widetilde{X}_j \right| \right]^2}{\sum\limits_{j=1}^{2} \left[\lim\limits_{t \to +\infty} \left| \Delta_L \widetilde{x}_j(t) \right| \right]^2} \right)^{\frac{1}{2}} \times 100\%, \tag{54}$$

$$J_2 = \left(\frac{\sum\limits_{j=1}^{2} \int\limits_{t_0-}^{(T_{\max})_j} \left[\widetilde{x}_j(t) - \Delta_L \widetilde{x}_j(t) - \widetilde{X}_j \right]^2 dt}{\sum\limits_{j=1}^{2} \int\limits_{t_0-}^{(T_{\max})_j} \left[\Delta_L \widetilde{x}_j(t) \right]^2 dt} \right)^{\frac{1}{2}} \times 100\%. \tag{55}$$

where $(T_{\max})_j$ is the upper limit of the integration. This upper limit is equal to the settling time of $x_j(t)$, which is a measurable variable that is around 2% of its steady-state value. The input in this computational experiment was selected to be of the following step form, which depends on the input operating value

$$u(t) = U(1 + p_u u_s(t - t_0)), \tag{56}$$

where $p_u \in [(p_u)_{\min}, (p_u)_{\max}]$ and where

$$-1 < (p_u)_{\min} < (p_u)_{\max} < (U_{\max}/U) - 1. \tag{57}$$

All cost functions in (53)–(55) are evaluated for various step amplitudes in (56) and initial conditions of the nonlinear model and compatible conditions of its linear approximant. The initial values of the nonlinear system are of the form $\widetilde{x}_j(t_0-) = (1 + p_j)\widetilde{X}_j$, where $p_j \in \left((p_j)_{\min}, (p_j)_{\max} \right)$, $(p_j)_{\min}, (p_j)_{\max} \in \mathbb{R}$, $j \in \{1, 2\}$ and

$$-1 < (p_j)_{\min} < (p_j)_{\max} < \left(\widetilde{X}_{j,\max}/\widetilde{X}_j \right) - 1. \tag{58}$$

For a given set of initial conditions and input signal, the linear approximant is declared as an accurate representation of the original nonlinear model (1) if

$$(J_1 < \varepsilon_1) \wedge (J_2 < \varepsilon_2) \wedge (J_\infty < \varepsilon_\infty). \tag{59}$$

where $\varepsilon_\infty, \varepsilon_1, \varepsilon_2 \in \mathbb{R}_+$ are desirable upper bounds for the metrics in (53)–(55) to be set by the designer.

Clearly, both nonlinear model (1) and linear approximant (2) are asymptotically stable. Hence, the metric J_1 defined in (54) does not depend upon the initial conditions but only upon the steady-state value of the actuatable input. After applying a series of algebraic manipulations, the metric J_1 is determined to have the following analytic form:

$$J_1 = 100\left|\frac{p_u U}{U(1+p_u) - \mu_m}\right|. \tag{60}$$

The computational experiments used to examine the accuracy of (2) compared with (1) were accomplished using the following values of the fermentation process (see [23,24]): $Y_{c/s} = 0.07$, $S_a = 100\,\text{g/L}$, $\mu_m = 0.38\,\text{h}^{-1}$ and $K_s = 0.5\,\text{g/L}$. With respect to the metric bounds, without loss of generality, let $\varepsilon_\infty = 5\,\%$, $\varepsilon_1 = 5\,\%$ and $\varepsilon_2 = 5\,\%$. The computational experiments were executed for different operating conditions and various values of p_u, p_1 and p_2. In particular, 37 scenarios of nominal conditions of the input were tested (see Table 1). Clearly, the above physical parameters and input nominal values uniquely determined the respective nominal values of the state variables using (42).

Table 1. Scenarios for the nominal values of the input.

n/n	U	n/n	U	n/n	U	n/n	U
1	0.0185	11	0.1827	21	0.2702	31	0.3213
2	0.0495	12	0.1936	22	0.2775	32	0.3249
3	0.0714	13	0.2046	23	0.2830	33	0.3286
4	0.0878	14	0.2137	24	0.2885	34	0.3322
5	0.1042	15	0.2228	25	0.2939	35	0.3359
6	0.1188	16	0.2319	26	0.2994	36	0.3395
7	0.1334	17	0.2410	27	0.3049	37	0.3432
8	0.1462	18	0.2483	28	0.3104		
9	0.1590	19	0.2556	29	0.3140		
10	0.1717	20	0.2629	30	0.3176		

The result of the computation experiment was the derivation of the areas satisfying the conditions in (59) for all 37 scenarios. Indicatively, in Figure 1, the accuracy areas for $p_j = 0$ ($j = 1, 2$) are presented. For each operating point, there existed a range of inputs and initial conditions that satisfied the conditions in (59). The overlapping depended upon the distance of input nominal values of adjacent scenarios. Note that as the nominal value of the input approached $U_{\max}$, the width of the accuracy areas decreased.

The derivation of the operating point scenarios was carried out through a series of computational experiments, verifying that the inequality constraints in (59) were satisfied for each operating point while there was minimal overlapping of the areas covering the entire area of nominal values of the input. Clearly, the determination of the operating points was not unique and depended upon the desired degree of overlapping. The linear approximant derived in the following sections was used to develop the switching bank of observers.

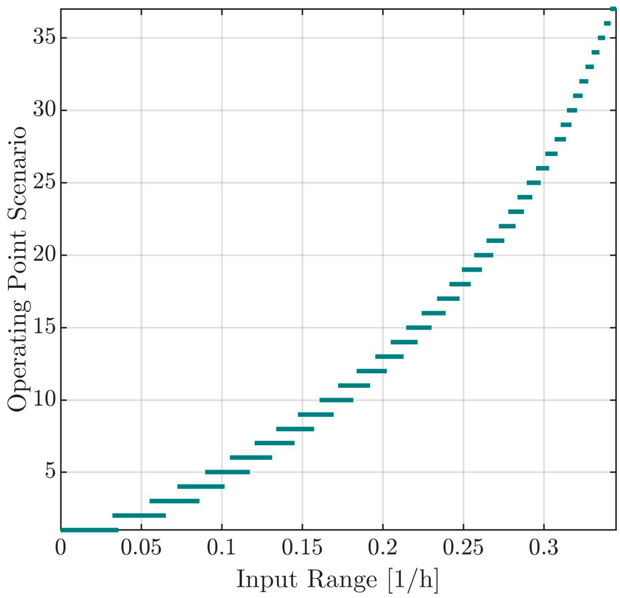

Figure 1. Operating point accuracy areas.

6. Full-Order Observer Design Based on the Linear Approximant of the Alcoholic Fermentation Nonlinear Model

In the present section, using the linear approximant of the alcoholic fermentation process presented in Section 5, a full-state observer is designed by expressing the general form of the observer matrices as functions of the linear approximant parameters and the degrees of freedom of the observer, satisfying appropriate nonlinear inequality constraints. The performance of the estimation results was illustrated through simulations.

6.1. Observer Design

In the present section, full-order observers for the estimation of $\Delta_L x(t)$ is designed. By applying elementary computations, it can be verified that the observability matrix of $\aleph_L$ is of the form

$$\mathbb{O} = \begin{bmatrix} 0 & 1 \\ -\frac{U}{Y_{c/s}} & -h_D - U \end{bmatrix}. \tag{61}$$

Considering that the nominal value of the input is constrained to satisfy (44), it can readily be observed that $\det\{\mathbb{O}\} \neq 0$ and hence $\aleph_L$ is observable. The general form of the full-order observer of the linear approximant of the system is of the form

$$\Im_L : \quad \begin{matrix} \Delta_L \dot{\hat{x}}(t) = F\Delta_L \hat{x}(t) + g\Delta_L y(t) + m\Delta u(t) \\ \Delta_L \hat{x}(0-) = \Delta_L \hat{x}_0 \end{matrix} \quad , \tag{62}$$

where $\Delta_L \hat{x}(t)$ is the estimation of the state vector of $\aleph_L$. The general forms of the observer matrices are

$$F = \begin{bmatrix} 0 & h_D Y_{c/s} - g_1 \\ -\frac{U}{Y_{c/s}} & -h_D - U - g_2 \end{bmatrix}, \; g = \begin{bmatrix} g_1 \\ g_2 \end{bmatrix}, \; m = b, \tag{63}$$

where $g_1, g_2 \in \mathbb{R}$. Clearly, the error dynamics of the observer are described by (13). The parameters g_1 and g_2 are to be selected by the designer under the constraint to satisfy the stability and desired error response characteristics of the error dynamics of the observer. From (63), it can be observed that the observer characteristic polynomial is of the form

$$p_o(s) = s^2 + a_{f,1}s + a_{f,0}, \tag{64}$$

where $a_{f,1} = g_2 + h_D + U$ and $a_{f,0} = \overline{u}(h_D - g_1/Y_{c/s})$. To achieve a small enough estimation error and desirable transient response characteristics, the regional stability of the observer characteristic polynomial (64) is imposed. In particular, consider the $a-$ regional stability requirement presented in Section 2. This property is satisfied if and only if

$$(g_2 > 2a - h_D - U) \wedge \left(g_1 < U^{-1}Y_{c/s}\left[a^2 + h_d U - a(g_2 + h_D + U)\right]\right). \tag{65}$$

From (65), it can be observed that the general solutions of the observer gains g_1 and g_2 are

$$g_1 = Y_{c/s}\left[h_D - aU^{-1}(a+\gamma_1) - \gamma_2\right], \tag{66}$$

$$g_2 = 2a - h_D - U + \gamma_1, \tag{67}$$

where $\gamma_1, \gamma_2 \in \mathbb{R}_+$ are free parameters. In addition to the requirement for regional stability, the requirement of real and distinct roots of the characteristic polynomial of F is also imposed. This additional requirement is satisfied if and only if $0 < \gamma_2 < \gamma_1^2/4U$. Clearly, the eigenvalues of F belong to $\mathbb{C}_a^-$ and are real and distinct if and only if

$$(\gamma_1 > 0) \wedge \left(0 < \gamma_2 < \frac{\gamma_1^2}{4U}\right). \tag{68}$$

Assuming that the inequalities in (48) hold, the observer matrix F takes on the form

$$F = F(\gamma_1, \gamma_2) = \begin{bmatrix} 0 & Y_{c/s}\left[aU^{-1}(a+\gamma_1) + \gamma_2\right] \\ -U/Y_{c/s} & -2a - \gamma_1 \end{bmatrix}, \tag{69}$$

while the coefficients of the polynomial in (64) become $a_{f,1} = 2a + \gamma_1$ and $a_{f,0} = a(a+\gamma_1) + U\gamma_2$. Using (18) and applying a series of computations, it can be observed that

$$\Phi_1 = \begin{bmatrix} \frac{-2a-\gamma_1+\sqrt{\gamma_1^2-4U\gamma_2}}{2\sqrt{\gamma_1^2-4U\gamma_2}} & -\frac{Y_{c/s}[a(a+\gamma_1)+U\gamma_2]}{U\sqrt{\gamma_1^2-4U\gamma_2}} \\ \frac{U}{Y_{c/s}\sqrt{\gamma_1^2-4U\gamma_2}} & \frac{2a+\gamma_1+\sqrt{\gamma_1^2-4U\gamma_2}}{2\sqrt{\gamma_1^2-4U\gamma_2}} \end{bmatrix}, \ \Phi_2 = I_2 - \Phi_1 \tag{70}$$

In what follows, it is assumed that $\alpha = 2$. Also, after applying appropriate manipulations, it can be verified that

$$\|\Phi_1\|_2^2 = \|\Phi_2\|_2^2 = \left\{\left(U^2 + a^2 Y_{c/s}^2\right)\left[U^2 + Y_{c/s}^2(a+\gamma_1)^2\right] - 2U^3 Y_{c/s}^2\gamma_2 + 2aUY_{c/s}^4(a+\gamma_1)\gamma_2 + U^2 Y_{c/s}^4\gamma_2^2\right\} / \left[U^2 Y_{c/s}^2\left(\gamma_1^2 - 4U\gamma_2\right)\right]. \tag{71}$$

Furthermore, it can be observed that

$$\left(J_{e,O}^*\right)_1 = \widetilde{J}_{SS,1}|u_w| \tag{72}$$

$$\left(J_{e,O}^*\right)_2 = \widetilde{J}_{SS,2}|u_w| \tag{73}$$

where

$$\widetilde{J}_{SS,1} = \left|\frac{\left[a^2 + a(\gamma_1 - 2U) + U(\gamma_2 - \gamma_1)\right]\left[(K_s + S_a)U - S_a\mu_m\right]}{U\left\{S_a U(U-\mu_m)^2 + K_s\left[U^3 - U^2\mu_m + a(a+\gamma_1)\mu_m + U(\gamma_2 - h_d)\mu_m\right]\right\}}\right| \tag{74}$$

$$\widetilde{J}_{SS,2} = \left|\frac{U\left[(K_s + S_a)U - S_a\mu_m\right]}{S_a U(U-\mu_m)^2 + K_s\left[U^3 - U^2\mu_m + a(a+\gamma_1)\mu_m + U(\gamma_2 - h_d)\mu_m\right]}\right| \tag{75}$$

From (72) and (75), it can be observed that

$$\frac{\left(J_{e,O}^*\right)_1}{\left(J_{e,O}^*\right)_2} = \frac{\widetilde{J}_{SS,1}}{\widetilde{J}_{SS,2}} = \frac{1}{U^2}\left|a^2 + a(\gamma_1 - 2U) + U(\gamma_2 - \gamma_1)\right| \tag{76}$$

For observer design purposes, it is desirable that the inequalities in (23) and (24) hold. The parameter u_w can be considered known a priori. Hence, the design inequalities in (23) and (24) can be restated as

$$\left(\widetilde{J}_{SS,1} \leq \widetilde{\zeta}_{SS,1}\right) \wedge \left(\widetilde{J}_{SS,2} \leq \widetilde{\zeta}_{SS,2}\right) \wedge (J_e \leq \zeta_e) \tag{77}$$

where $\widetilde{\zeta}_{SS,1}, \widetilde{\zeta}_{SS,2} \in \mathbb{R}_+$ are to be selected by the designer.

Assuming that the inequalities in (68) hold and setting

$$\gamma_1 = -2a + \rho_{F,1} + \rho_{F,2},\ \gamma_2 = (a - \rho_{F,1})(a - \rho_{F,2})/U, \tag{78}$$

the observer matrices are rewritten in terms of the observer poles as

$$F = F(\rho_{F,1}, \rho_{F,2}) = \begin{bmatrix} 0 & Y_{c/s}\rho_{F,1}\rho_{F,2}/U \\ -U/Y_{c/s} & -(\rho_{F,1} + \rho_{F,2}) \end{bmatrix}, \tag{79}$$

$$g = g(\rho_{F,1}, \rho_{F,2}) = \begin{bmatrix} \frac{Y_{c/s}\left[S_a U (U-\mu_m)^2 + K_s\left(U^3 - U^2\mu_m - \mu_m\rho_{F,1}\rho_{F,2}\right)\right]}{K_s U \mu_m} \\ -\frac{U^2}{\mu_m} - \frac{S_a (U-\mu_m)^2}{K_s \mu_m} + \rho_{F,1} + \rho_{F,2} \end{bmatrix}. \tag{80}$$

Furthermore, the two norms of Φ_1 and Φ_2, as well as $\widetilde{J}_{SS,1}$ and $\widetilde{J}_{SS,2}$, take on the form

$$\|\Phi_1\|_2^2 = \|\Phi_2\|_2^2 = \frac{\left(U^2 + Y_{c/s}^2\rho_{F,1}^2\right)\left(U^2 + Y_{c/s}^2\rho_{F,2}^2\right)}{U^2 Y_{c/s}^2 (\rho_{F,1} - \rho_{F,2})^2}, \tag{81}$$

$$\widetilde{J}_{SS,1} = \frac{(K_s + S_a)U - S_a\mu_m}{K_s U \mu_m \rho_{F,1}\rho_{F,2}} |U(\rho_{F,1} + \rho_{F,2}) - \rho_{F,1}\rho_{F,2}|, \tag{82}$$

$$\widetilde{J}_{SS,2} = \frac{U[(K_s + S_a)U - S_a\mu_m]}{K_s \mu_m \rho_{F,1}\rho_{F,2}}. \tag{83}$$

Using (51), the relations in (80), (82) and (83) take on the form

$$g = g(\rho_{F,1}, \rho_{F,2}) = \begin{bmatrix} Y_{c/s}\left(h_D - \frac{\rho_{F,1}\rho_{F,2}}{U}\right) \\ \rho_{F,1} + \rho_{F,2} - h_D - U \end{bmatrix}, \tag{84}$$

$$\widetilde{J}_{SS,1} = \frac{h_D}{U(\mu_m - U)\rho_{F,1}\rho_{F,2}} |U(\rho_{F,1} + \rho_{F,2}) - \rho_{F,1}\rho_{F,2}|, \tag{85}$$

$$\widetilde{J}_{SS,2} = \frac{h_D U}{(\mu_m - U)\rho_{F,1}\rho_{F,2}}. \tag{86}$$

Using (81), (85) and (86), it can be verified that the conditions in (77) are satisfied if and only if

$$\left(\widetilde{\zeta}_{SS,1} \geq \left(\widetilde{\zeta}_{SS,1}\right)_{\min}(h_D, \rho_{F,1}, \rho_{F,2})\right) \wedge \left(\widetilde{\zeta}_{SS,2} \geq \left(\widetilde{\zeta}_{SS,2}\right)_{\min}(h_D, \rho_{F,1}, \rho_{F,2})\right) \wedge (\zeta_e \geq (\zeta_e)_{\min}(\rho_{F,1}, \rho_{F,2})). \tag{87}$$

where

$$\left(\widetilde{\zeta}_{SS,1}\right)_{\min}(h_D, \rho_{F,1}, \rho_{F,2}) = h_D \frac{U(\rho_{F,1} + \rho_{F,2}) - \rho_{F,1}\rho_{F,2}}{U(U - \mu_m)\rho_{F,1}\rho_{F,2}}, \tag{88}$$

$$\left(\widetilde{\zeta}_{SS,2}\right)_{\min}(h_D, \rho_{F,1}, \rho_{F,2}) = \frac{h_D U}{(\mu_m - U)\rho_{F,1}\rho_{F,2}}, \tag{89}$$

$$(\zeta_e)_{\min}(\rho_{F,1}, \rho_{F,2}) = 2\sqrt{\frac{e^{-2a}\left(U^2 + Y_{c/s}^2\rho_{F,1}^2\right)\left(U^2 + Y_{c/s}^2\rho_{F,2}^2\right)}{U^2 Y_{c/s}^2 (\rho_{F,1} - \rho_{F,2})^2}}. \tag{90}$$

Without loss of generality, let $\rho_{F,2} = \lambda\rho_{F,1}$, where $\lambda > 1$. By applying a series of computations to (88), it can be verified that

$$\inf_{\substack{\rho_{F,1} \in (a,\infty) \\ \lambda \in (1,\infty)}} \left(\tilde{\zeta}_{SS,1}\right)_{\min}(h_D, \rho_{F,1}, \rho_{F,2}) = \begin{cases} \frac{h_D(a-2U)}{aU(\mu_m - U)} & \text{if } a \in (2U, +\infty) \\ 0 & \text{if } a \in (0, 2U] \end{cases}. \tag{91}$$

It can also be verified that the minimum value of the upper branch of (91) is achieved as $\rho_{F,1}$ tends to a and λ tends to unity, i.e., it holds that

$$\lim_{\substack{\rho_{F,1} \to a \\ \lambda \to 1}} \left(\tilde{\zeta}_{SS,1}\right)_{\min}(h_D, \rho_{F,1}, \rho_{F,2}) = \frac{h_D(a-2U)}{aU(\mu_m - U)}, \tag{92}$$

while the lower branch of (91) is achieved for

$$\rho_{F,1} = U(1+\lambda)/\lambda, \tag{93}$$

In a similar manner, from (89), it can be verified that

$$\inf_{\substack{\rho_{F,1} \in (a,\infty) \\ \lambda \in (1,\infty)}} \left(\tilde{\zeta}_{SS,2}\right)_{\min}(h_d, \rho_{F,1}, \rho_{F,2}) = 0. \tag{94}$$

while the minimum value of (89) is achieved for $\lambda\rho_{F,1}^2$ tending to infinity.

Finally, applying a series of computations to (90), it can be observed that

$$\inf_{\substack{\rho_{F,1} \in (a,\infty) \\ \lambda \in (1,\infty)}} (\zeta_e)_{\min}(\rho_{F,1}, \rho_{F,2}) = 2e^{-a}\frac{\lambda+1}{\lambda-1} \tag{95}$$

if

$$\left(1 < \lambda \le \frac{U^2}{a^2 Y_{c/s}^2}\right) \wedge \left(0 < a < \frac{U}{Y_{c/s}}\right) \tag{96}$$

or

$$\inf_{\substack{\rho_{F,1} \in (a,\infty) \\ \lambda \in (1,\infty)}} (\zeta_e)_{\min}(\rho_{F,1}, \rho_{F,2}) = \frac{2e^{-a}}{aUY_{c/s}(\lambda-1)}\sqrt{\left(U^2 + a^2Y_{c/s}^2\right)\left(U^2 + a^2Y_{c/s}^2\lambda^2\right)} \tag{97}$$

if

$$\left[\left(\lambda > \frac{U^2}{a^2Y_{c/s}^2}\right) \wedge \left(0 < a < \frac{U}{Y_{c/s}}\right)\right] \vee \left[(\lambda > 1) \wedge \left(a \ge \frac{U}{Y_{c/s}}\right)\right] \tag{98}$$

With respect to the stability margin of the observer poles, three distinct cases are examined. In the first case, the observer poles are considered to depend upon the operating point, namely, it is required that the stability margin is greater than the linear approximant system poles corresponding to the operating point at hand, while it is not necessary to simultaneously cover all scenarios of nominal values of the input. In this case, the respective stability margin is chosen to satisfy the following inequality

$$a_i > \max\{U_i, h_D(U_i)\}. \tag{99}$$

Note that

$$\max\{U_i, h_D(U_i)\} = \begin{cases} h_D(U_i) & \text{if } U_i < \mu_m\left(1 - \sqrt{\frac{K_s}{K_s+S_a}}\right) \\ U_i & \text{if } \mu_m\left(1 - \sqrt{\frac{K_s}{K_s+S_a}}\right) < U_i < \mu_m \end{cases}. \tag{100}$$

Considering that the system poles depend upon the nominal value of the input, in order to cover all valid scenarios of the nominal value of the input, it suffices to set the stability margin to satisfy the inequality

$$a > \sup_{U \in (0, U_{\max})} \{\max\{U, h_D(U)\}\}. \tag{101}$$

This is the second scenario for the stability margin. By applying a series of computations, it can be verified that

$$\sup_{U \in (0, U_{\max})} \{\max\{U, h_D(U)\}\} = \frac{S_a \mu_m}{K_s}. \tag{102}$$

In the third stability margin scenario, which is of particular interest, the observer poles are determined such that the steady-state error between the biomass concentration and the estimation of biomass concentration for step input changes equals zero, i.e.,

$$J_{SS,1} = 0. \tag{103}$$

Applying elementary computations, it can be verified that the condition in (103) can be satisfied if and only if

$$\rho_{F,1} = U_i(1+\lambda)/\lambda. \tag{104}$$

Considering that $\lambda > 1$, it can readily be verified that $\rho_{F,1} > U_i$. Assuming that $\max\{U_i, h_D(U_i)\} = U_i$, using an appropriate choice of λ, the inequality in (99) can be satisfied under the constraint

$$a_i \in (U_i, 2U_i). \tag{105}$$

Assuming that $\max\{U_i, h_D(U_i)\} = h_D(U_i)$, two cases can be distinguished. By applying a series of computations, it can be observed that if

$$(U_i < h_D(U_i) < 2U_i) \wedge \left(1 < \lambda < \frac{U_i}{h_D(U_i) - U_i}\right). \tag{106}$$

then the inequality in (99) is satisfied. Note that the first inequality in (106) is satisfied if and only if

$$\frac{\mu_m}{2(K_s + S_a)}\left[3K_s + 2S_a - \sqrt{K_s(9K_s + 8S_a)}\right] < U_i < \mu_m\left(1 - \sqrt{\frac{K_s}{K_s + S_a}}\right). \tag{107}$$

Assuming that the constraints in (106) are not satisfied, then the inequality in (99) cannot be satisfied by any choice of λ. Nevertheless, if

$$\left[(U_i < h_D(U_i) \leq 2U_i) \wedge \left(\lambda > \frac{U_i}{h_D(U_i) - U_i}\right)\right] \vee \left[(h_D(U_i) > 2U_i) \wedge \left(\lambda > \frac{h_D(U_i) - U_i}{U_i}\right)\right], \tag{108}$$

it can be verified that

$$(\rho_{F,1} > U_i) \wedge (\lambda \rho_{F,1} > h_D(U_i)). \tag{109}$$

Clearly, since $\lambda > 1$, it can be verified that $a_i = U_i(1+\lambda)/\lambda$.

6.2. Determination of the Observer Parameters

From Section 6.1, it is observed that the analytic determination of λ and $\rho_{F,1}$ is complicated, as $J_{SS,1}$, $J_{SS,2}$ and J_e are nonlinear functions of the observer parameters. Consequently, the problem of determining observer parameters so that the inequalities in (77) are simultaneously satisfied can be studied using a heuristic type of algorithm.

As already mentioned in Section 6.1, of particular interest is the case where the steady-state error between the biomass concentration and the estimation of biomass concentration for step input changes equals zero, which is achieved using (104). For observer design purposes, it remains to determine λ so that the second and third inequalities in (77) are satisfied. To avoid numerical errors in the implementation of the observer, the value of λ must be as small as possible. By applying a series of computations upon the second inequality in (77), it can be observed that

$$|u_w| \le Q_2(\lambda). \tag{110}$$

where

$$Q_2(\lambda) = \frac{\zeta_{SS,2} U_i (1+\lambda)^2 (\mu_m - U_i)}{h_d \lambda}. \tag{111}$$

Using elementary manipulations, it can be observed that its first derivative is

$$Q_2^{(1)}(\lambda) = \frac{dQ_2(\lambda)}{d\lambda} = \frac{U_i(\lambda^2-1)\zeta_{SS,2}(\mu_m - U_i)}{h_d \lambda^2}. \tag{112}$$

From (112) it can be verified that $Q_2^{(1)}(\lambda)$ is strictly increasing for all $\lambda \in (1,\infty)$. Similarly, the third inequality in (77) can be rewritten as

$$Q_3(\lambda) \le \zeta_e \tag{113}$$

where

$$Q_3(\lambda) = \frac{2\exp\left[-U_i\left(1+\frac{1}{\lambda}\right)\right]}{Y_{c/s}(\lambda^2-1)} \sqrt{\left[1+Y_{c/s}^2(1+\lambda)^2\right]\left[\lambda^2+Y_{c/s}^2(1+\lambda)^2\right]} \tag{114}$$

Applying elementary computations to (114), it can be observed that

$$Q_3^{(1)}(\lambda) = \frac{dQ_3(\lambda)}{d\lambda} =$$

$$\frac{2U(\lambda^2-1)\left[1+Y_{c/s}^2(1+\lambda)^2\right]\left[\lambda^2+Y_{c/s}^2(1+\lambda)^2\right] - 2\lambda^2\left[\lambda+Y_{c/s}^2(1+\lambda)^2\right]\left[1+\lambda^2+2Y_{c/s}^2(1+\lambda)^2\right]}{Y_{c/s}\lambda^2(\lambda^2-1)^2\sqrt{\left[1+Y_{c/s}^2(1+\lambda)^2\right]\left[\lambda^2+Y_{c/s}^2(1+\lambda)^2\right]}} e^{-U_i(1+\frac{1}{\lambda})} \tag{115}$$

From (115), it can be verified that $Q_3^{(1)}(\lambda)$ is strictly decreasing for all $\lambda \in (1,\infty)$.

For observer design purposes, it is desirable for $Q_2(\lambda)$ to be greater than or equal to a desired value so that the bounds of u_w also increase. Let u_w^* be the desired upper bound of u_w. Considering that $Q_2(\lambda)$ is strictly increasing and that $\lim_{\lambda\to\infty} Q_2(\lambda) = \infty$, the desired bound is achieved for $\lambda = \lambda_2^*$ so that $Q_2(\lambda_2^*) = u_w^*$ or equivalently that

$$\lambda_2^* = \frac{h_D u_w^* + \sqrt{h_d}\sqrt{u_w^*}\sqrt{h_d u_w^* + 4U_i\zeta_{SS,2}(U_i-\mu_m)} + 2U\zeta_{SS,2}(U_i-\mu_m)}{2U\zeta_{SS,2}(\mu_m - U_i)} \tag{116}$$

Similarly, it is desirable for $Q_3(\lambda)$ to satisfy the third inequality in (77). Considering that $Q_3(\lambda)$ is strictly decreasing and that $\lim_{\lambda\to\infty} Q_3(\lambda) = 2e^{-U_i}\sqrt{1+Y_{c/s}^2}$, the desired bound is achieved for $\lambda = \lambda_3^*$ so that

$$Q_3(\lambda_3^*) = \zeta_e \tag{117}$$

where $\zeta_e > \lim_{\lambda\to\infty} Q_3(\lambda)$.

The coefficient λ is selected to be

$$\lambda_i = \max\{\lambda_2^*, \lambda_3^*\} \tag{118}$$

It is important to mention that setting u_w and assuming that the model parameters are perfectly known, the number of target areas that are needed to satisfy the dense web principle can be determined a priori.

6.3. Simulation Results

In this subsection, the performance of the proposed observer scheme is demonstrated for the 30th scenario of the nominal value of the input presented in Table 1, as well as the model parameters presented in Section 2.3. For simulation purposes, it was assumed that $\rho_{F,1}$ satisfied relation (93), while $\lambda = 100$. Regarding the initial conditions of the nonlinear system and the observer it was assumed that $\tilde{x}(0-) = \begin{bmatrix}\tilde{X}_1 & \tilde{X}_2\end{bmatrix}^T$, $\Delta_L x(0-) = \begin{bmatrix}0 & 0\end{bmatrix}^T$ and $\Delta_L \hat{x}(0-) = \begin{bmatrix}-0.05\tilde{X}_1 & 0\end{bmatrix}^T$. Finally, the actuatable input signal was considered to be of the form $u(t) = U(1 + 0.1u_s(t))$. In Figures A1 and A2, the nonlinear and linear approximant model responses are presented in comparison with the respective observer responses, while in Figures A3 and A4, the respective estimation errors are presented. With respect to the first state variable, i.e., the non-measurable variable, for both nonlinear and linear approximant cases (see Figures A1 and A3), the estimation error tended to zero. With respect to the second state variable, i.e., the measurable variable, it can be observed that the linear approximant estimation tended to the linear approximant response, resulting in zero steady-state error (see Figures A2 and A4). In contrast, for the nonlinear case, a small steady-state error appeared. The steady-state error appeared due to the difference between the nonlinear and linear approximant model responses and depended upon the selection of the parameter λ. It can be verified that the steady-state error for the second state variable was inversely proportional to λ (see also Figure A5). It is important to mention that having λ equal to 100, leading to the derivation of the simulations in the present subsection, was chosen in order to guarantee that the steady state estimation error between the observer and the nonlinear model of the system was well below 5 %.

It is important to mention that the above simulation results were derived as if the linear approximant parameters were known. In the following section, a full-order observer, where its parameters are derived through identification, is presented.

7. Full-Order Observer Design Using Parameter Identification

In the present section, the full-order observer scheme proposed in Section 6 for the estimation of the state variables of the alcoholic fermentation process is extended so that its parameters are determined using identification. The identification of the model parameters is carried out by appropriately exciting the process with a rich enough actuation signal. For the procedure to be more realistic, additive noise is also considered. For all nominal point scenarios presented in Section 5.2, the success of the identification procedure was verified.

7.1. Observer Design Using Identified Parameters

The identification is accomplished using experimental measurement data of the deviations of $y(t)$ and $u(t)$ around an operating point (Y, U). Clearly, U is known and Y can be derived through experimentation. Therefore, $\Delta y(t)$ and $\Delta u(t)$ are known. According to (5), the identified I/O linear model around (Y, U) is

$$\mathfrak{S}_I: \ \ \Delta y^{(1)}(t) + \hat{h}_D \Delta y(t) = \hat{h}_N \Delta u(t) + \varepsilon_I(t). \tag{119}$$

Substitution of the identified values of the coefficients in (119) to the observer matrices yields

$$F\left(\hat{h}_D, g_1, g_2\right) = \begin{bmatrix} 0 & \hat{h}_D Y_{c/s} - g_1 \\ -\frac{U}{Y_{c/s}} & -\hat{h}_D - U - g_2 \end{bmatrix}, \ m(\hat{h}_N) = \begin{bmatrix} -Y_{c/s}\hat{h}_N \\ \hat{h}_N \end{bmatrix}. \tag{120}$$

Following (66) and (67), the measurement output gains of the observer take on the form

$$g_1 = Y_{c/s}\left[\hat{h}_D - aU^{-1}(a+\gamma_1) - \gamma_2\right], \tag{121}$$

$$g_2 = 2a - \hat{h}_D - U + \gamma_1, \tag{122}$$

From (120) and (122), it can be verified that F and, consequently, the coefficients of its characteristic polynomial are independent of the identified coefficients. Using relation (79) and (80), the observer matrices can be rewritten in terms of the observer poles.

7.2. Alcoholic Fermentation Parameter Identification

In all scenarios of nominal values presented in Table 1, the system excitation is of the form

$$u(t) = U_i + \lambda_{p,i} f_p(t) + \lambda_{O,i} f_0(t);\ i = 1, \ldots, 37, \tag{123}$$

where U_i is the nominal value of the input for the nominal operating point scenario i; $\lambda_{p,i}$ and $\lambda_{O,i}$ are real scaling factors; $f_p(t)$ is a zero-mean periodic pulse signal with pulse period τ_p and percentile pulse width w_p; and $f_0(t)$ is a linear chirp signal, i.e., a sinusoidal wave whose frequency varies linearly from an initial value f_s to a final value f_f from $t \in [0, T_{\max}]$ (indicatively see Figures A6 and A7). For all scenarios of the nominal value of the input, it was assumed that $\tau_p = 60$ h, $w_p = 50\%$, $f_s = 0.2\,\mathrm{h}^{-1}$, $f_f = 0.01\,\mathrm{h}^{-1}$ and $T_{\max} = 300\,\mathrm{h}$. With respect to the gains $\lambda_{p,i}$ and $\lambda_{O,i}$, for all scenarios of the nominal values of the input, they were considered to be 15 % and 5 % of the half-width of the accuracy area of the nominal value of the input, respectively.

As already mentioned, an additive measurement noise of the white Gaussian form with a signal-to-noise ratio equal to 80 was considered to be applied. The identification algorithm uses a combination of (a) the subspace Gauss–Newton least-squares search algorithm, (b) the Levenberg–Marquardt least-squares search algorithm, (c) the adaptive subspace Gauss–Newton search and (d) the steepest descent least-squares search algorithm, where each algorithm is tried in sequence at each iteration. The first direction leading to a reduction in estimation cost is used (see [40]). By applying a series of computational experiments, the identification results presented in Table A1 were derived. From Table A1, it can readily be observed that in all cases, the estimated values $\hat{h}_D$ and $\hat{h}_N$ were extremely close to the respective values derived from the linear approximants. Furthermore, the mean squared error, the final prediction error and the percentile fit of the response of the identified model to the estimation data suggest minimal deviation between the identified and the linear approximant models. From the numerical results presented in Table A1, it can readily be deduced that the estimated linear approximant parameters were extremely near the respective parameters, which were analytically determined using the linear approximant, and that the simulated results found using the identified coefficients fit the original signals very well in the sense that they produced almost visually identical time plots. It is important to mention that the success of the identification procedure highly depends upon the amplitude of the actuation signal. Higher amplitudes may result in a linear approximant not being an accurate representation of the nonlinear system, leading to deviations in the estimated parameters.

8. Performance of the Switching Observer Scheme for the Alcoholic Fermentation Process

In the present section, the performance of the overall switching/identification/metaheuristic scheme for the alcoholic fermentation process is investigated. In particular, it was assumed that it was desired to at least cover an input nominal value area $U \in [U_L, U_U]$, where $U_L = 0.083\,\mathrm{h}^{-1}$ and $U_U = 0.317\,\mathrm{h}^{-1}$. The area between U_L and U_U was divided into seven equally distanced operating points, corresponding to the nominal values of inputs and state variables presented in Table 2. For the determination of the observer parameters, the following was desirable:

- The dense web principle between adjacent operating areas was achieved with 10% overlapping between the areas (see Figure 2).
- The steady-state error between the biomass concentration and the estimation of biomass concentration was equal to zero.
- The convergence rate metric was bounded through the third inequality in (77) assuming that $\zeta_e = 1.1 \lim_{\lambda_i \to \infty} Q_3(\lambda_i)$, depending upon the operating point.

Considering the model parameters presented in Section 5.3, the observer parameters were determined using relations (104) and (118).

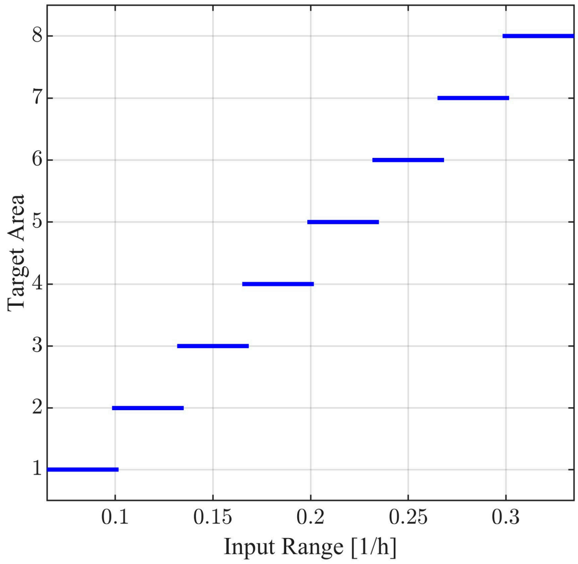

Figure 2. Target operating areas.

Table 2. Operating points.

n/n	U_i	$\widetilde{X}_{1,i}$	$\widetilde{X}_{2,i}$
1	0.083	6.990	0.140
2	0.116	6.984	0.222
3	0.150	6.977	0.326
4	0.183	6.967	0.466
5	0.217	6.954	0.663
6	0.250	6.933	0.962
7	0.283	6.897	1.466
8	0.317	6.825	2.500

Clearly, in order to evaluate the observer matrices, for each operating point in Table 2, the estimation of h_D and h_N needed to be performed for each operating point. To do so, the procedure described in Section 7.2 was used. For all scenarios of the nominal value of the input, it was assumed that $\tau_p = 60\,\mathrm{h}$, $w_p = 50\,\%$, $T_{\max} = 300\,\mathrm{h}$, $\lambda_{p,i} = 0.005U_i$ and $\lambda_{O,i} = 0.0002U_i$. Note that $\lambda_{p,i}$ and $\lambda_{O,i}$ were selected to be quite small in order to practically guarantee that for each operating point, the linear approximant model of the fermentation process was an accurate representation of the original nonlinear model around the respective operating point.

With respect to the chirp signal initial and final frequencies f_s and f_f, they must be determined such that they highlight the dynamics of the process for each operating point. In order to determine the meaningful frequencies for each operating point, experimental determination of Bode magnitude plots was carried out. The experimental procedure was based on actuating the nonlinear system with sinusoidal inputs around an operating point and determining the peak-to-peak fluctuation of the measurable output for various frequencies. The Bode plot amplitude for each frequency was determined through the ratio of the output peak-to-peak oscillation divided by the amplitude of the sinusoidal part of the input signal (see Figure 3). In what follows, f_s was chosen to be the frequency above which the amplitude of the output oscillation was lower than 1% of the maximum oscillation determined for frequencies lower than f_s. In Table 3, the identification results for each operating point and the corresponding parameters λ are presented. From Table 3, it can readily be verified that the estimations of the I/O transfer function parameters were very near the analytically determined values and that the simulated measurable output signals fit the measurable data extremely well. With respect to the observer parameter λ, it can be verified that its value varied significantly between the operating points.

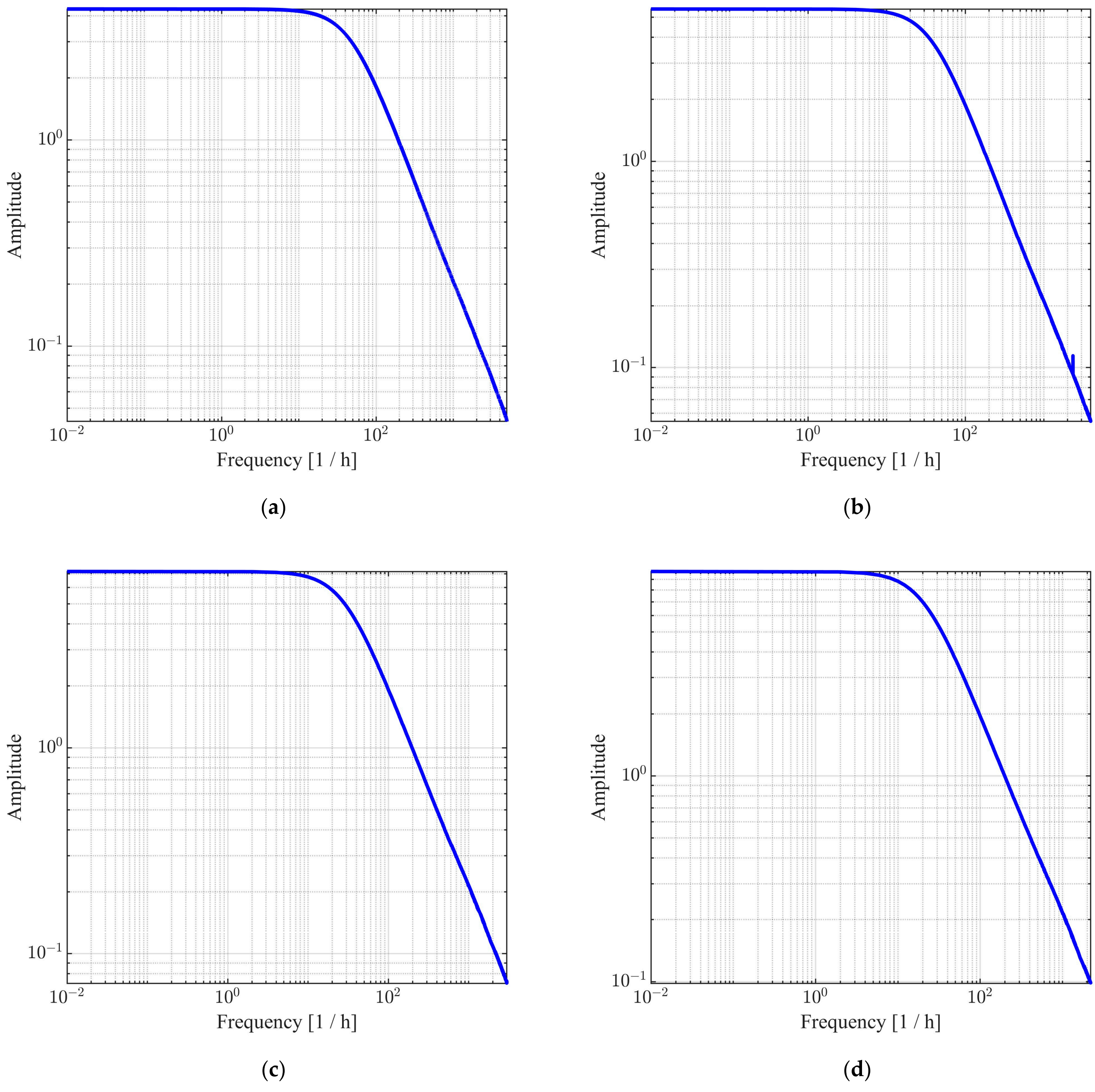

Figure 3. *Cont.*

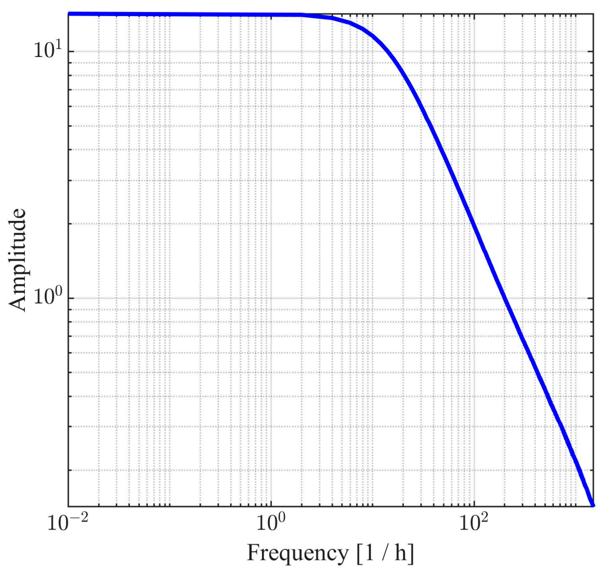

(**e**)

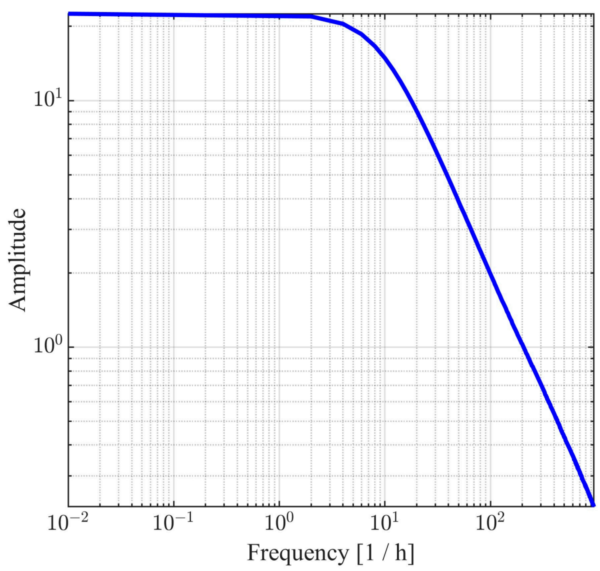

(**f**)

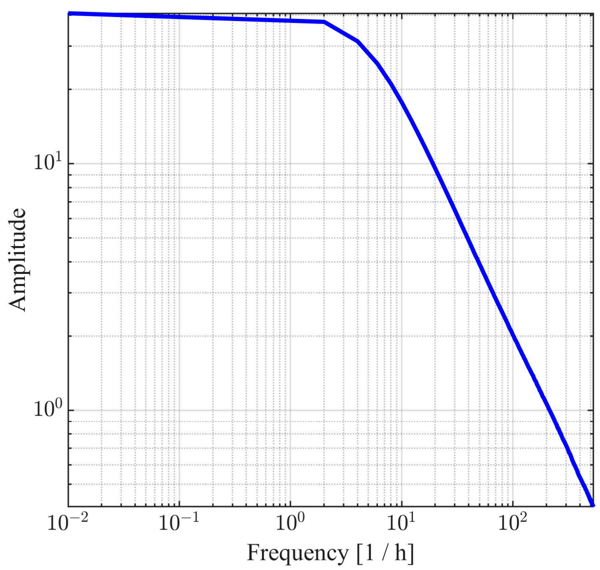

(**g**)

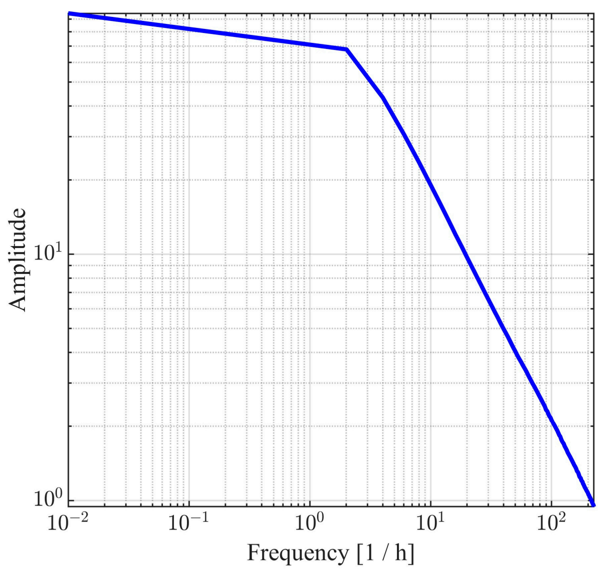

(**h**)

Figure 3. Bode amplitude plots for all nominal input scenarios: (**a**) scenario 1, (**b**) scenario 2, (**c**) scenario 3, (**d**) scenario 4, (**e**) scenario 5, (**f**) scenario 6, (**g**) scenario 7 and (**h**) scenario 8.

The transitions through target operating areas started from an initial operating point $\ell_I = (Y_I, U_I)$ and settled at the final operating point $\ell_D = (Y_D, U_D)$, passing through the intermediate destination points $\ell_{D,j} = (Y_{D,j}, U_{D,j})$ $(j = 1, \ldots, 6)$. The point ℓ_I belonged to target area 1. The points $\ell_{D,j} = (Y_{D,j}, U_{D,j})$ $(j = 1, \ldots, 6)$ belonged to target areas 2 to 7, respectively. Finally, $\ell_{D,7}$ and ℓ_D belonged to target area 8. In all cases, the time where each transition was triggered was chosen to be 10% greater than the settling time of the respective linear approximant. Also, let

$$\begin{gathered} Y_I = 0.1213\,\mathrm{g/L},\ Y_{D,1} = 0.1786\,\mathrm{g/L},\ Y_{D,2} = 0.2703\,\mathrm{g/L},\ Y_{D,3} = 0.3906\,\mathrm{g/L}, \\ Y_{D,4} = 0.5556\,\mathrm{g/L},\ Y_{D,5} = 0.7955\,\mathrm{g/L},\ Y_{D,6} = 1.1765\,\mathrm{g/L},\ Y_{D,7} = 1.8750\,\mathrm{g/L}, \\ Y_D = 3.0077\,\mathrm{g/L},\ U_I = 0.0742\,\mathrm{h}^{-1},\ U_{D,1} = 0.1\,\mathrm{h}^{-1},\ U_{D,2} = 0.1333\,\mathrm{h}^{-1},\ U_{D,3} = 0.1667\,\mathrm{h}^{-1}, \\ U_{D,4} = 0.2\,\mathrm{h}^{-1},\ U_{D,5} = 0.2333\,\mathrm{h}^{-1},\ U_{D,6} = 0.2667\,\mathrm{h}^{-1},\ U_{D,7} = 0.3\,\mathrm{h}^{-1},\ U_D = 0.3258\,\mathrm{h}^{-1}. \end{gathered}$$

Table 3. Identified model and observer parameters.

n/n	U_i	h_D	$\hat{h}_D$	h_N	$\hat{h}_N$	PF	MSE	λ
1	0.083	46.26	46.42	99.86	100.20	98.43 %	1.9865×10^{-10}	1719.06
2	0.117	36.42	36.50	99.78	100.00	98.61 %	4.9157×10^{-10}	1086.98
3	0.150	27.75	27.79	99.67	99.81	98.79 %	1.0688×10^{-9}	736.38
4	0.183	20.26	20.26	99.53	99.53	98.96 %	2.1689×10^{-9}	513.09
5	0.217	13.95	13.94	99.34	99.30	99.14 %	4.3879×10^{-9}	359.12
6	0.250	8.81	8.80	99.04	98.97	99.31 %	9.2627×10^{-9}	246.28
7	0.283	4.85	4.84	98.53	98.43	99.49 %	2.1530×10^{-8}	159.98
8	0.317	2.06	2.05	97.50	97.28	99.66 %	6.2573×10^{-8}	91.79

In Figure 4a,b, the response of the nonlinear system and the switching observer scheme are presented, while in Figure 5a,b, the respective estimation errors are presented. From Figure 4a,b, it can readily be observed that the estimation of the biomass concentration and the substrate concentration are visually identical to the respective nonlinear model responses, presenting small estimation errors (see Figure 5a,b). It is important to mention that the proposed switching approach performed significantly better than a single-step non-switching approach from ℓ_I to ℓ_D, also presented in Figure 4a,b. It can readily be observed that the estimations of the state variables were highly inaccurate, also presenting significant steady-state error.

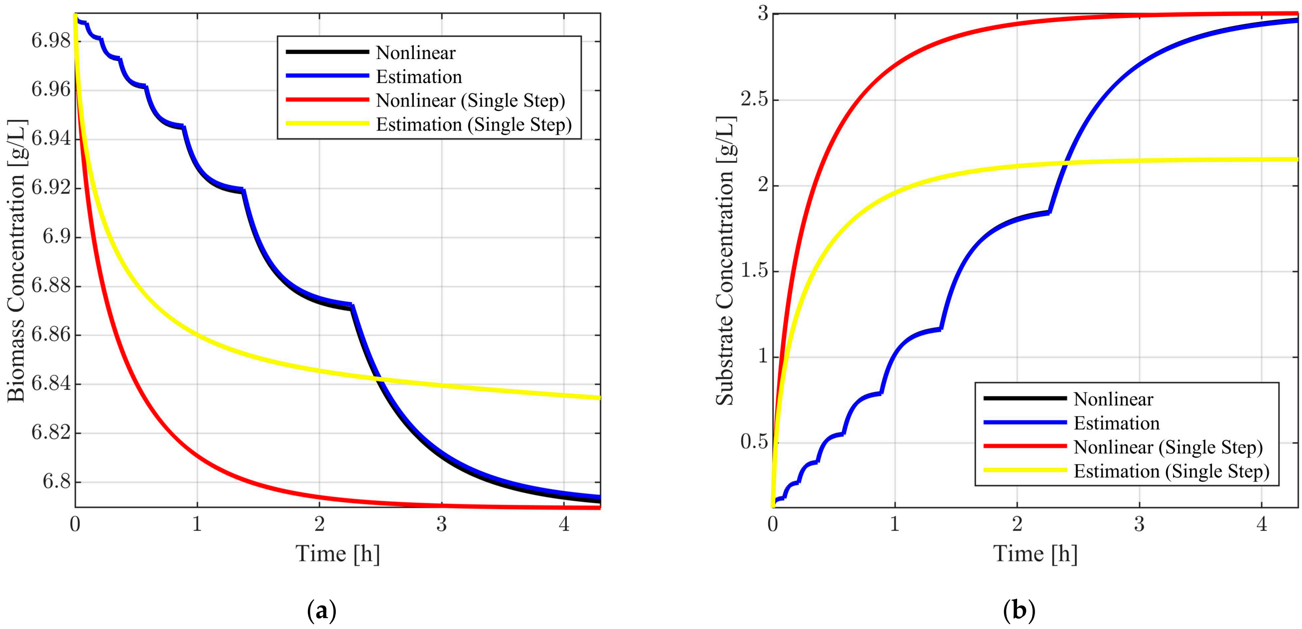

Figure 4. State variable response estimations: (**a**) biomass concentration and (**b**) substrate concentration.

It is important to mention that the performance of the switching scheme depends upon the number of steps from the initial to the final destination point. The smallest number of steps was 1, where the process was driven to move from the initial to the destination point in a single step. As already mentioned, in Figure 4, it can readily be verified that that the single-step approach failed to provide an accurate estimation of the system variables during the transient phenomenon, as well as in the steady state. In order to examine the influence of the number of steps, consider the observer accuracy metric

$$\delta_j\left(x_j, \hat{x}_j\right) = 100\% \times \left\|x_j(t) - \hat{x}_j(t)\right\|_2 / \left\|x_j(t) - x_j(t_0-)\right\|_2, \; j = 1,2 \tag{124}$$

where

$$\|\delta(t)\|_2^2 = \int_{t_0-}^{T_{\max}} \delta(t)^2 dt; \; T_{\max} > t_0-$$

After a series of computational experiments, for 2 to 8 steps of transition between ℓ_I and ℓ_D, the metrics in (124) are presented in Table 4. It can readily be observed that especially for the non-measurable variable, as the number of steps decreased, the performance of the observer scheme deteriorated significantly.

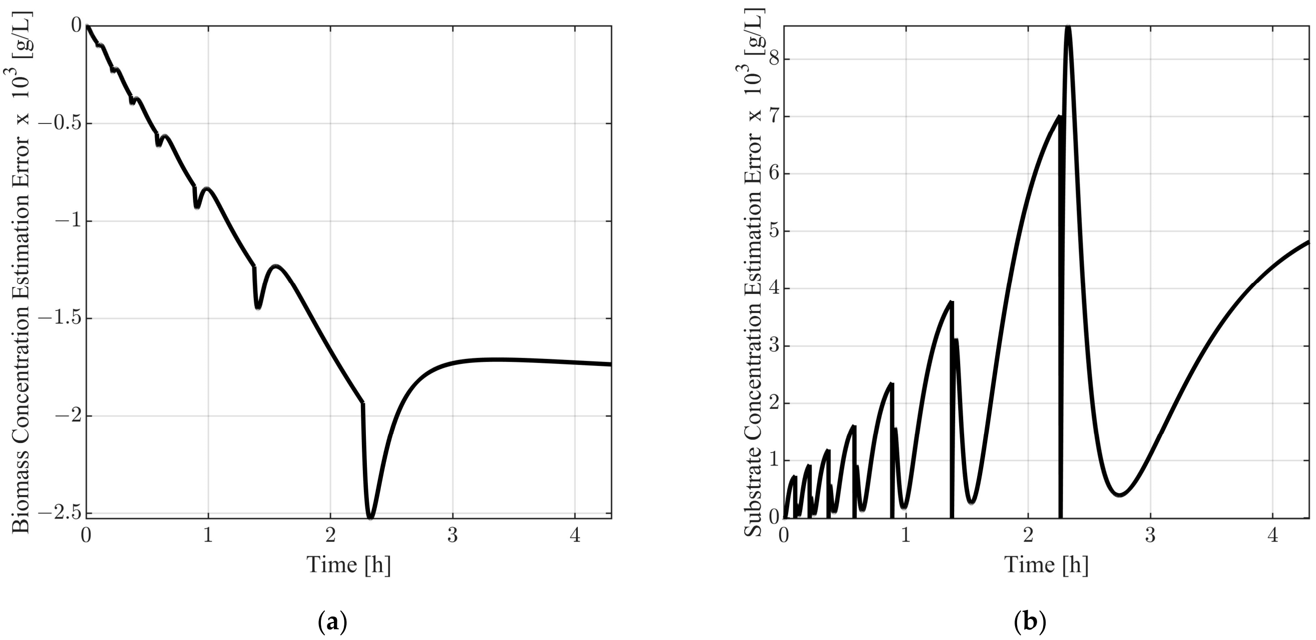

Figure 5. State variable response estimation errors: (**a**) biomass concentration estimation error and (**b**) substrate concentration estimation error.

Table 4. Accuracy metrics of the switching scheme for various numbers of steps.

Steps	$\boldsymbol{\delta_1}$	$\boldsymbol{\delta_2}$
2	154.1738 %	1.8305 %
3	41.2932 %	1.3010 %
4	14.2551 %	0.9744 %
5	5.7663 %	0.7610 %
6	2.6250 %	0.4777 %
7	1.4388 %	0.2858 %
8	1.0209 %	0.1744 %

It is important to mention that the switching observer scheme behaved satisfactorily, even in the presence of measurement noise for the substrate concentration. In order to demonstrate the scheme's resilience to the presence of noise, for the same simulation experiment presented previously (see Figures 4 and 5), the estimated values of the state variables of the system in the presence of noise will be compared with the noise-free response of the nonlinear system. The noise was considered to be an additive random signal of the form

$$f_{n,i}(t) = p\widetilde{X}_{2,i}\widetilde{f}_{n,i}(t) i = 1, \ldots, 8 \tag{125}$$

where $\widetilde{f}_{n,i}(t) : \mathbb{R}_+ \to [-1, 1]$ and where p is an appropriate scaling factor. The form of the noise signal in (125) implied that the amplitude of the noise increased as the scheme switched to higher nominal values of the substrate concentration. The signal $\widetilde{f}_{n,i}(t)$ was generated using an appropriate random discrete time signal fed to a zero-order-hold D/A and a continuous time filter. For simulation purposes, it was assumed that the discrete time signal had a sampling period of $T_s = 0.01$ h, while the filter's transfer function was of the form

$$h_f(s) = \frac{1}{\left(T_{f,1}s + 1\right)\left(T_{f,2}s + 1\right)} \tag{126}$$

where $T_{f,1} = 0.0002$ and $T_{f,2} = 0.0003$. In what follows, the estimations of the biomass concentration and the substrate concentration are compared with the respective noise-free nonlinear system responses using (124). By applying a series of computations, it can be observed (see Figures 6 and 7) that the estimations remained accurate, even in the presence of large noise signals.

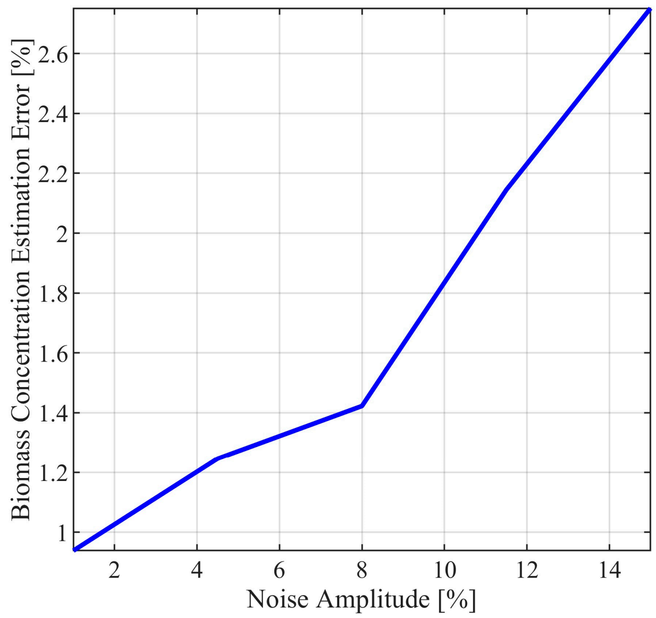

Figure 6. Biomass concentration accuracy for various amplitudes of the measurement noise.

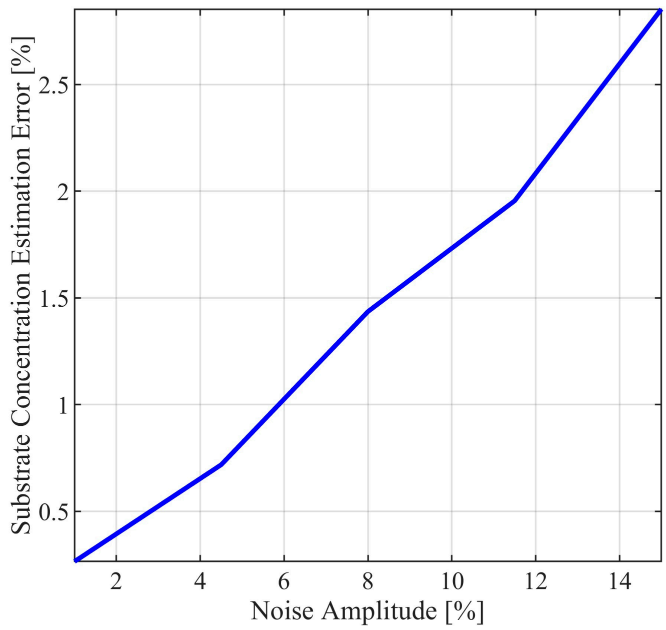

Figure 7. Substrate concentration accuracy for various amplitudes of the measurement noise.

It is important to mention that the observer parameter selection can be accomplished using the metaheuristic algorithm described in Section 3. Consider the nominal points of the input presented in Table 3, with the respective identified coefficients $\hat{h}_D$ and $\hat{h}_N$ and a desired $|u_w| = 0.0183\ \mathrm{h}^{-1}$, as in the analytic approach described previously. With respect to the metaheuristic algorithm, it was assumed that $n_{loop} = 200$, $n_{rep} = 20$, $n_{tot} = 10^6$, $\sigma = 0.001$,$(\widetilde{\rho}_{F,1})\left(\hat{h}_i, U_i\right) = U_i$, $\left(\widehat{\rho}_{F,1}\right)\left(\hat{h}_i, U_i\right) = 20U_i$, $(\widetilde{\rho}_{F,2})\left(\hat{h}_i, U_i\right) = U_i$, $\left(\widehat{\rho}_{F,2}\right)\left(\hat{h}_i, U_i\right)$ =2000U_i, ${}^{i}\zeta_{SS,1} = 0.02$, ${}^{i}\zeta_{SS,2} = 0.02$ and ${}^{i}\zeta_e = 2.2e^{-U_i}\sqrt{1 + Y_{c/s}^2}$. The gains in relation (26a) were chosen to be as shown in Table 5.

Table 5. Performance criterion gains.

$\gamma_{e,A}$	$(\gamma_{e,O})_1$	$(\gamma_{e,O})_2$	$(\gamma_F)_1$	$(\gamma_F)_2$	γ_w
0	0.95	0	0	0.05	0

The choice of the numerical values in Table 5 suggests that the design goal of the metaheuristic algorithm focuses on (a) the minimization of the steady state estimation error of the non-measurable system variable, which is the main goal of the soft sensor, and (b) the appropriate boundness of the observer poles. Regarding (b), it is recalled that the observer poles are constrained such that $0 < \rho_{F,1} < \rho_{F,2}$. Hence, for both observer poles to be appropriately bounded, it suffices to bound only $\rho_{F,2}$. Thus, the cost corresponding to an appropriate bound of $\rho_{F,1}$ can be neglected by choosing $(\gamma_F)_1 = 0$. Since the amplitude of the input was set a priori, the gain γ_w was chosen to be equal to zero. Clearly, the cost corresponding to the steady state error of the measurable output variable, which is important in fault detection, did not have any essential influence on the satisfactory estimation of the non-measurable variable. Therefore, to reveal the value of the cost criterion corresponding to the steady-state error of the non-measurable variable, the weight factor $(\gamma_{e,O})_2$ was chosen to be equal to zero. The choice of the remaining gains was made using preliminary computational experiments using different values of the gains that revealed their influence on the performance criterion. Regarding the cost corresponding to the free response of the estimation error model, the computational experiments showed that it was neglectable. Thus, $\gamma_{e,A}$ was chosen to be equal to zero. The remaining metaheuristic algorithm parameters were evaluated by considering the computational complexity of the algorithm and the time needed for each repetition to be completed. The bounds ${}^i\zeta_{SS,1}$, ${}^i\zeta_{SS,2}$ and ${}^i\zeta_e$ were determined so that the steady state and transient behavior of the observer had desirable characteristics.

In each loop of the metaheuristic algorithm, the generated observer parameter data are considered to be valid if the inequalities in (11), (23) and (24) are satisfied and $(U_i < \rho_{F,1} < \rho_{F,2}) \wedge \left(\hat{h}_{D,i} < \rho_{F,2}\right)$. The results of the metaheuristic process are summarized in Table 6. Defining the convergence metric

$$\sigma^* = \max\left\{\left|\frac{(\rho_{F,1})_w\left(\hat{h}_i, U_i\right)}{(\rho_{F,1})_c\left(\hat{h}_i, U_i\right)}\right|, \left|\frac{(\rho_{F,2})_w\left(\hat{h}_i, U_i\right)}{(\rho_{F,2})_c\left(\hat{h}_i, U_i\right)}\right|, \left|\frac{(u_w)_w}{(u_w)_c}\right|\right\} \tag{127}$$

it can be observed that for all nominal values of the input, the metaheuristic algorithm converged to the observer parameters, satisfying the design requirements. The switching scheme simulation results were also similar to those produced using the analytic determination of the observer parameters presented earlier (see Figures 8 and 9). Note that the metaheuristic approach seemed to present improved performance with respect to the estimation error of the non-measurable variable (see Figures 5a and 9a), which was almost one order of magnitude smaller.

Table 6. Metaheuristic algorithm results.

n/n	U_i	$\rho_{F,1}$	$\rho_{F,2}$	Q	$\left(J^*_{e,O}\right)_1$	$\left(J^*_{e,O}\right)_2$	$J^*_{e,A}$	σ^*
1	0.083	0.0834289	142.998	1022.42	0.0193277	0.0199999	1.84557	0.000222579
2	0.116	0.116869	126.599	801.365	0.0175970	0.0199997	1.78558	0.000933145
3	0.150	0.150408	110.258	607.836	0.0199614	0.0199997	1.72763	0.000189896
4	0.183	0.184046	93.899	440.851	0.0197554	0.0199994	1.67182	0.000287858
5	0.217	0.217877	77.6684	301.620	0.0199265	0.0199995	1.61825	0.000434413
6	0.250	0.252035	61.4591	188.861	0.0198582	0.0199994	1.56736	0.000447879
7	0.283	0.2869	45.2447	102.355	0.0199558	0.0199989	1.52059	0.000436400
8	0.317	0.323656	29.0092	42.0772	0.0199964	0.0199999	1.48480	0.000158437

In the above parameter selection procedure, the half-width of the target operating area $|u_w|$ is considered known and preset. Clearly, the metaheuristic algorithm presented in Section 3 can be appropriately adjusted to also determine the half-width of the target operating area. Indicatively, choosing the weight factors of the performance criterion in (30) as shown in Table 7, setting $\sigma = 0.02$ and keeping the remaining metaheuristic algorithm parameters as shown in the previous experiment, the simulation results presented in Table 8 were produced using the metaheuristic algorithm. The first, third and fourth weight factors in (30) were chosen following Table 5, while the rest were chosen using preliminary computational experiments. From Table 8, it can be observed that the dense web principle was satisfied and that no superfluous points corresponding to target areas covered by other ones existed (see Figure 10). Clearly, the widths of the first and second target areas were smaller than those set in the previous cases, while for the remaining areas, the respective width gradually increased to reach the last target area width, which was more than double in size. The switching scheme simulation results were also similar to those produced using the analytic determination of the observer parameters or the first metaheuristic scheme presented earlier (see Figures 11 and 12). Note that the estimation of the state variables of the alcoholic fermentation process were visually identical to the respective nonlinear model responses.

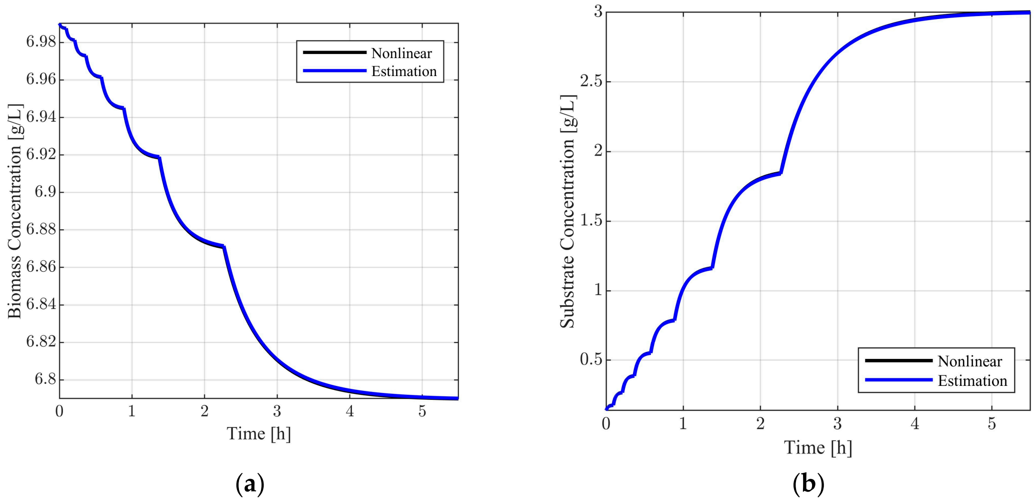

Figure 8. State variable response estimations: (**a**) biomass concentration and (**b**) substrate concentration.

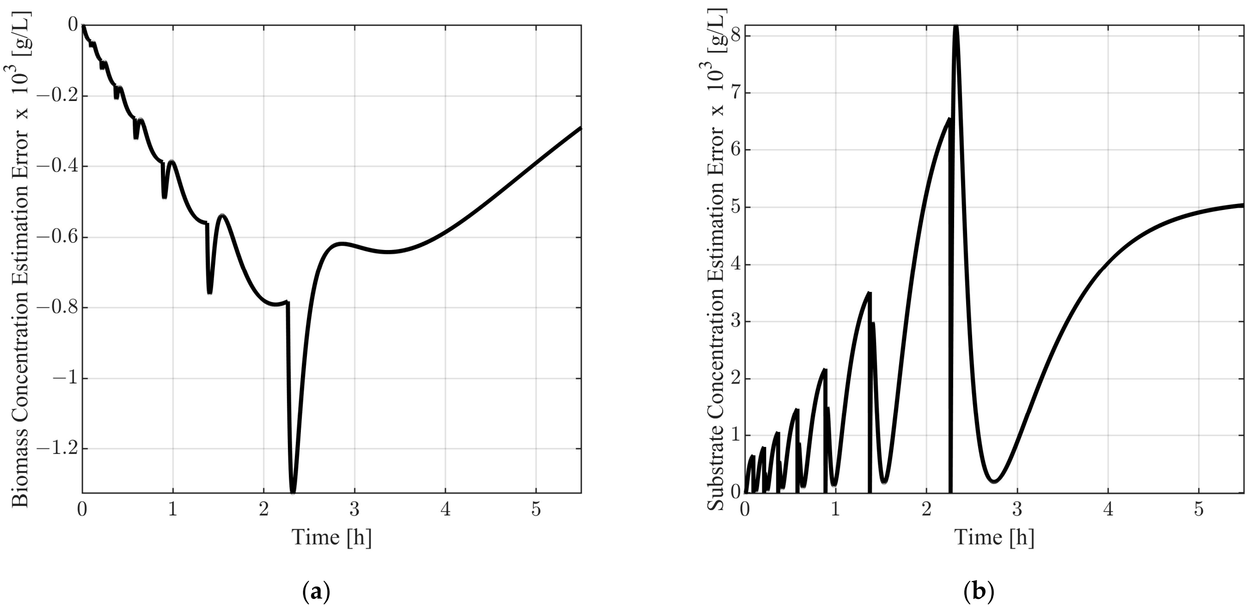

Figure 9. State variable response estimation errors: (**a**) biomass concentration estimation error and (**b**) substrate concentration estimation error.

Table 7. Performance criterion gains.

$\gamma_{e,A}$	$(\gamma_{e,O})_1$	$(\gamma_{e,O})_2$	$(\gamma_F)_1$	$(\gamma_F)_2$	γ_w
0	0.45	0	0	0.01	0.45

Table 8. Metaheuristic algorithm results.

n/n	U_i	$\rho_{F,1}$	$\rho_{F,2}$	$\lvert u_w \rvert$	Q	$\left(J^*_{e,O}\right)_1$	$\left(J^*_{e,O}\right)_2$	$J^*_{e,A}$	σ^*
1	0.083	0.083436	128.729	0.016475	3314.942	0.018047	0.019999	1.845688	0.019541
2	0.116	0.116888	120.623	0.017437	2935.03	0.01922	0.019997	1.785641	0.015009
3	0.150	0.150392	113.537	0.018841	2556.689	0.01954	0.019999	1.727569	0.016454
4	0.183	0.183974	103.767	0.020216	2177.875	0.01947	0.019999	1.67151	0.019001
5	0.217	0.217655	95.099	0.022383	1802.562	0.019967	0.019999	1.617334	0.01823
6	0.250	0.251471	84.450	0.025087	1428.219	0.019624	0.019997	1.565218	0.01912
7	0.283	0.285556	72.482	0.029176	1054.011	0.019977	0.019997	1.515246	0.017544
8	0.317	0.320105	58.3145	0.036382	680.0276	0.019772	0.019999	1.46821	0.018953

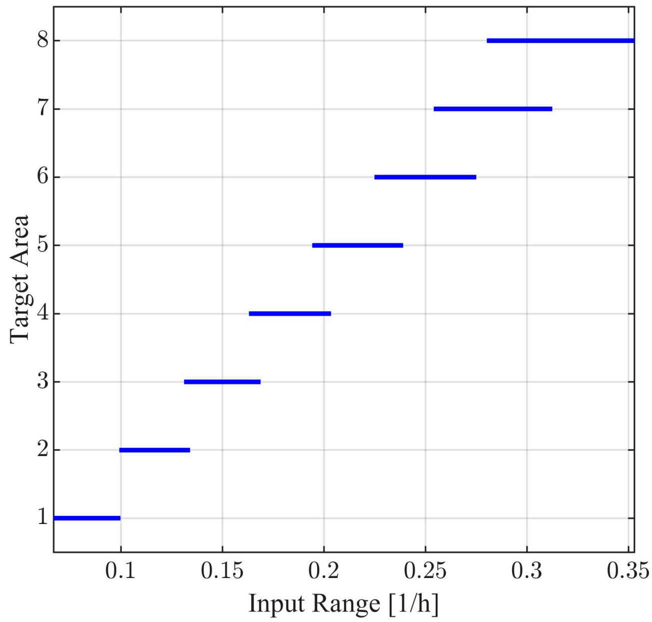

Figure 10. Target operating areas.

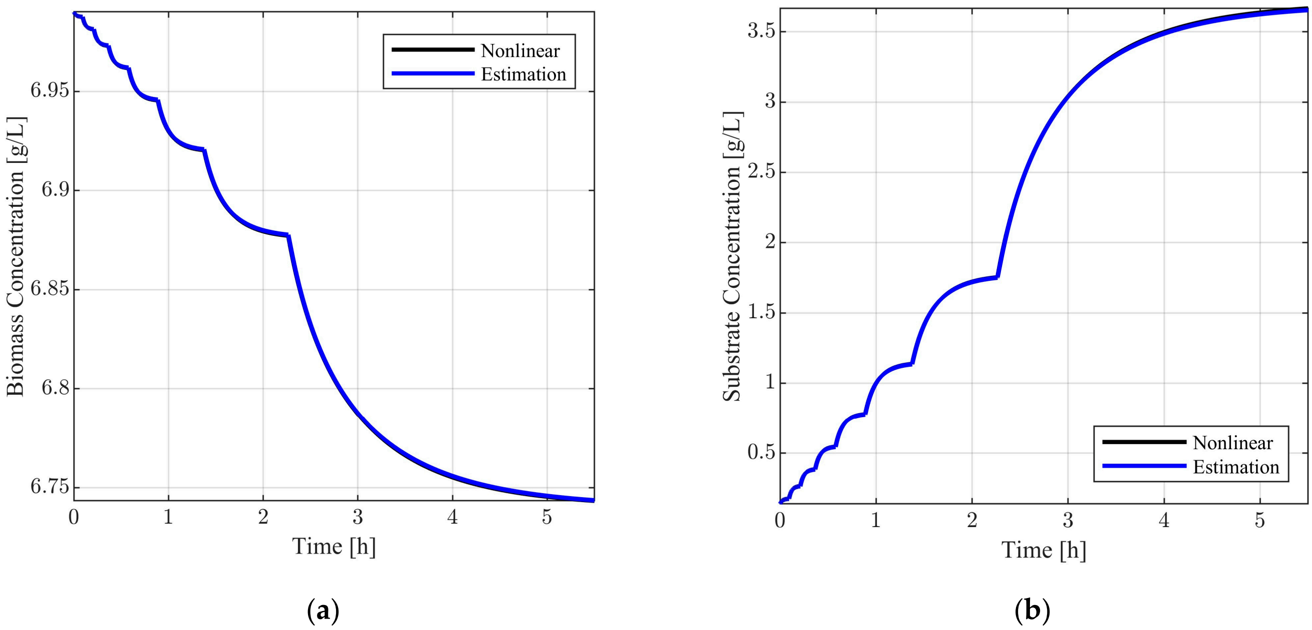

Figure 11. State variable response estimations: (**a**) biomass concentration and (**b**) substrate concentration.

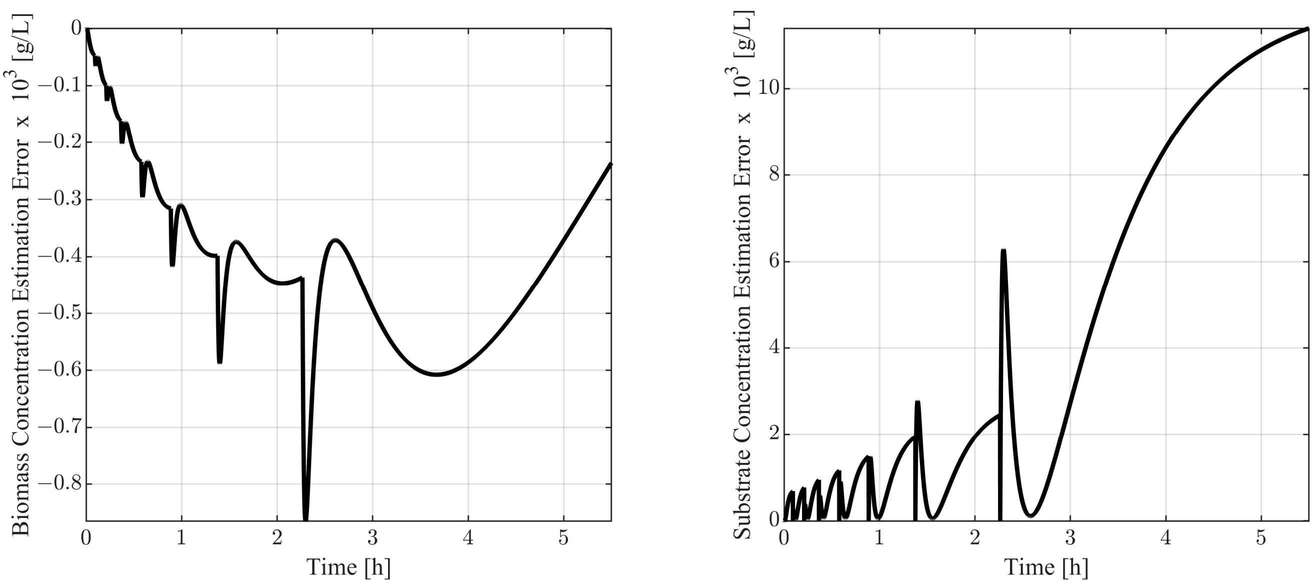

(**a**) (**b**)

Figure 12. State variable response estimation errors: (**a**) biomass concentration estimation error and (**b**) substrate concentration estimation error.

9. Conclusions

In the present study, following a set of assumptions, the improvement of the performance of soft sensors using switching observers was investigated through the development of an extended soft sensor design approach, including AI procedures. In particular, two metaheuristic procedures were developed. The procedures were based on the linear approximant of a nonlinear dynamic SISO system, and a linear full-order observer using system identification data. The basic assumption was the satisfaction of the property of I/O reconstructability of the state space linear approximant. Based on these two procedures, the switching procedure between observers in a bank of observers was accomplished, where the width of the target operating areas could be increased.

The results were successfully applied to the mathematical model of an alcoholic fermentation process. Based on the nonlinear model of the process, a linear approximant was produced and its accuracy compared with the original nonlinear mathematical representation was investigated using a series of computational experiments. Based on the linear approximant of the process, the respective observer was designed. The linear approximant model parameters were derived through the identification of different operating points upon the nonlinear model. Through computational experiments, it was verified that the responses of the linear identified models were near the respective responses of the nonlinear model. With respect to the determination of the observer parameters, three distinct cases were examined. In the first case, a purely analytic approach was used. In the second case, the widths of the target operating areas were selected a priori and the algorithm was used to determine the observer poles. Finally, in the third case, both observer parameters and the widths of the target operating areas were determined using the metaheuristic algorithm. In all cases, the switching observer scheme resulted in accurate estimations of the state variables of the system, even in the presence of measurement noise.

The present metaheuristic approach was expected to operate satisfactorily in the complex case of multi-input multi-output (MIMO) systems. Future perspectives of the present research include the following:

a. The alternation of some system assumptions.
b. The cover of the cases where the actuator and sensor faults take place.
c. The investigation of alternative suboptimal minimization algorithms for the performance of the switching observer, like simulated annealing algorithms [41–43] and genetic algorithms [44–46].
d. The development of switching observer-based controllers for the regulation of the performance variables of the system (see [47,48]).

Author Contributions: Conceptualization, N.D.K. and F.N.K.; methodology, N.D.K., F.N.K. and D.G.F.; software, N.D.K. and G.F.F.; validation, F.N.K. and G.F.F.; formal analysis, N.D.K. and F.N.K.; investigation, F.N.K. and G.F.F.; resources, D.G.F. and G.F.F.; data curation, D.G.F. and G.F.F.; writing—original draft preparation, N.D.K., F.N.K. and G.F.F.; writing—review and editing, F.N.K. and G.F.F.; visualization, N.D.K.; supervision, F.N.K.; project administration, N.D.K. and F.N.K. All authors have read and agreed to the published version of the manuscript.

Funding: This research received no external funding.

Data Availability Statement: All necessary data are either provided in the main body of the article or in the cited literature.

Conflicts of Interest: The authors declare no conflict of interest.

Nomenclature

Symbol	**Definition**
$\widetilde{x}$	State vector of the nonlinear SISO system
u	Nonlinear model actuatable input
y	Nonlinear model measurable output
$\widetilde{x}_0$	Initial value of the nonlinear model state vector
f_{NL}	Nonlinear vector function
c_{NL}	Nonlinear function mapping the state variables to the measurable output
$\widetilde{X}$	Nominal value of the state vector
U	Nominal value of the input
Y	Nominal value of the measurable output
h_{NL}	Function mapping the nominal value of the input to the nominal value of the output
ℓ	Pair of nominal values of the input and the corresponding nominal value of the output
$\mathbb{H}_L$	The set of all admissible ℓ values
$\Delta\widetilde{x}$	Deviation of the nonlinear model state vector from its nominal value
Δu	Deviation of the nonlinear model actuatable input from its nominal value
Δy	Deviation of the nonlinear model measurable output from its nominal value
c	Output matrix of the nonlinear model
$\aleph$	Linear approximant of the nonlinear SISO system
Δx_L	Approximant of the deviation $\Delta\widetilde{x}$
Δy_L	Approximant of the deviation Δy
$\Delta x_{L,0}$	Initial value of Δx_L
A	Linear approximant state matrix
b	Linear approximant input matrix
$\mathfrak{S}$	I/O approximant of the state space linear approximant
$\chi^{(k)}$	kth derivative of χ with respect to time
n_c	Rank of the controllability matrix of the linear approximant
h	I/O approximant coefficient vector
$h_{D,j}$	jth I/O approximant output signal coefficient
$h_{N,j}$	jth I/O approximant input signal coefficient
$\mathfrak{S}_I$	I/O linear approximant system expressed in terms of the identified coefficients
$\hat{h}$	I/O approximant identified coefficient vector
$\hat{h}_D$	Output signal identified coefficient vector
$\hat{h}_N$	Input signal identified coefficient vector
$\hat{h}_{D,j}$	jth element of $\hat{h}_D$
$\hat{h}_{N,j}$	jth element of $\hat{h}_N$
ε_I	Modeling error through identification
$\mathfrak{I}$	Full-order observer depending upon the identified system parameters
F	Observer state matrix
m	Observer input matrix
g	Observer measurable output matrix
C_a^-	Regional stability condition
s	Laplace transform variable
a	Stability margin

ρ_F	Vector of the eigenvalues of observer matrix F
$\rho_{F,j}$	jth element of ρ_F
ε_x	Modeling error between the nonlinear model and the linear approximant
e_O	Observer estimation error
$e_{O,0}$	Initial value of the observer estimation error
$e_{O,A}$	Free response of the observer estimation error
$e_{O,B}$	Forced response of the observer estimation error
Φ_k	Transition matrix of the observer corresponding to the kth element of ρ_F
u_s	Unit step signal
u_w	Change of the input amplitude during stepwise transition
$\varepsilon_{x,SS}$	Steady-state value of the modeling error
$\widetilde{X}_w$	Nominal values of the state variables after the application of the step input signal
$e_{O,SS}$	Steady-state estimation error
$\Vert\bullet\Vert_\alpha$	α norm of the argument quantity
$J^*_{e,A}$	Free response estimation error magnitude metric
ζ_e	Free response estimation error magnitude metric bound
$\left(J^*_{e,O}\right)_j$	Steady-state estimation error magnitude metric for the jth state variable
$\zeta_{SS,j}$	Steady-state estimation error magnitude metric bound for the jth state variable
$\vert\bullet\vert$	Absolute value of the argument signal
L	Set of nominal operating points of the process
ℓ_i	ith element of L
Y_i	Nominal value of the measurable output corresponding to ℓ_i
U_i	Nominal value of the input corresponding to ℓ_i
$\widetilde{X}_i$	Nominal value of the state vector corresponding to ℓ_i
$\aleph_i$	Linear approximant around ℓ_i
A_i	State matrix of the linear approximant around ℓ_i
b_i	Input matrix of the linear approximant around ℓ_i
c_i	Output matrix of the linear approximant around ℓ_i
μ	Number of elements in L
$\hat{h}_i$	Estimation of the I/O approximant coefficient vector around ℓ_i
${}^i\rho_F$	Vector of the eigenvalues of observer matrix F designed around ℓ_i
$\Im_i$	Observer designed around ℓ_i
ℓ_I	Initial operating point
Y_I	Nominal value of the output corresponding to ℓ_I
U_I	Nominal value of the input corresponding to ℓ_I
$\widetilde{X}_I$	Nominal value of the state vector corresponding to ℓ_I
ℓ_D	Destination operating point
Y_D	Nominal value of the output corresponding to ℓ_D
U_D	Nominal value of the input corresponding to ℓ_D
$\widetilde{X}_D$	Nominal value of the state vector corresponding to ℓ_D
$\mathbb{T}$	Target area of an operating point
${}^i\mathbb{T}_O$	Areas of U_I and U_D where the free response and steady-state metrics satisfy the respective bounds
$u_{i,\max}$	Maximum deviation around U_i defining the target area
${}^i\zeta_e$	Free response estimation error magnitude metric bound corresponding to ℓ_i
${}^i\zeta_{SS,j}$	Steady-state estimation error magnitude metric bound for the jth state variable corresponding to ℓ_i
$\gamma_{e,A}$	Non-negative real weight factor for $J^*_{e,A}$
$(\gamma_{e,O})_j$	Non-negative real weight factor for $\left(J^*_{e,O}\right)_j$
$(\gamma_F)_j$	Non-negative real weight factor for $\rho_{F,j}$
γ_w	Non-negative real weight factor for ${}^iu_w$
${}^iu_w$	Half-width of the target operating area
${}^i\widetilde{u}_w$	Minimum value of the search area for ${}^iu_w$
${}^i\widehat{u}_w$	Maximum value of the search area for ${}^iu_w$
$\left({}^iu_w\right)_w$	Width of the search area for ${}^iu_w$

$\left({}^{i}u_{w}\right)_{c}$	Center value of the search area for ${}^{i}u_{w}$
$\left(\widetilde{\rho}_{F,j}\right)$	Minimum value of the search area for $\rho_{F,j}$
$\left(\widehat{\rho}_{F,j}\right)$	Maximum value of the search area for $\rho_{F,j}$
$\left(\rho_{F,j}\right)_{w}$	Width of the search area for $\rho_{F,j}$
$\left(\rho_{F,j}\right)_{c}$	Center value of the search area for $\rho_{F,j}$
$\Im$	Search area of the observer parameters
n_{loop}	Number of loops of the metaheuristic algorithm
n_{rep}	Number of repetitions of the metaheuristic algorithm
n_{total}	Maximum allowable number of computations in the metaheuristic algorithm
σ	Metaheuristic algorithm convergence metric
Q	Metaheuristic algorithm performance criterion
$\delta\rho_{F,j}$	Range of suboptimal values $\rho_{F,j}$ after a set of n_{rep} repetitions has been performed
${}^{i}\delta u_{w}$	Range of suboptimal values ${}^{i}u_{w}$ after a set of n_{rep} repetitions has been performed
$U^{*}_{\max}$	Maximum value of the input area that must be covered through target operating areas
$U^{*}_{\min}$	Minimum value of the input area that must be covered through target operating areas
n_{p}	Initial number of nominal values
C	Biomass concentration
S	Substrate concentration
S_{a}	Influent substrate concentration
μ_{b}	Biomass growth rate
μ_{m}	Maximum growth rate
K_{s}	Saturation constant
$Y_{c/s}$	Yield coefficient
J_{∞}	Infinity-norm type accuracy metric
J_{1}	1-norm type accuracy metric
J_{2}	2-norm type accuracy metric
$(T_{\max})_{j}$	Settling time of the jth state variable
p_{u}	Input percentile change
$(p_{u})_{\min}$	Minimum value of p_{u}
$(p_{u})_{\max}$	Maximum value of p_{u}
p_{j}	Deviation of the initial condition of the jth state variable from the nominal value
ε_{∞}	J_{∞} bound
ε_{1}	J_{1} bound
ε_{2}	J_{2} bound
$\mathbb{O}$	Observability matrix
γ_{j}	jth free observer parameter
I_{j}	$j \times j$ identity matrix
λ	Observer pole ratio
$\lambda_{p,i}$	Pulse signal scaling factor
$\lambda_{O,i}$	Chirp signal scaling factor
f_{p}	Zero-mean periodic pulse signal
f_{0}	Linear chirp signal
τ_{p}	Time period of f_{p}
w_{p}	Pulse width of f_{p}
f_{s}	Starting frequency of the chirp signal
f_{f}	Ending frequency of the chirp signal
$T_{\max}$	Simulation time
PF	Percentile fit
MSE	Mean square error
FPE	Final prediction error
δ_{j}	jth variable estimation accuracy metric
$f_{n,i}$	Noise signal
$\widetilde{f}_{n,i}$	Continuous time random signal of unity amplitude
p	Noise signal scaling factor
h_{f}	Filter transfer function

$T_{f,j}$	jth noise filter parameter
T_s	Discrete time signal generator period

Appendix A. Simulation Results

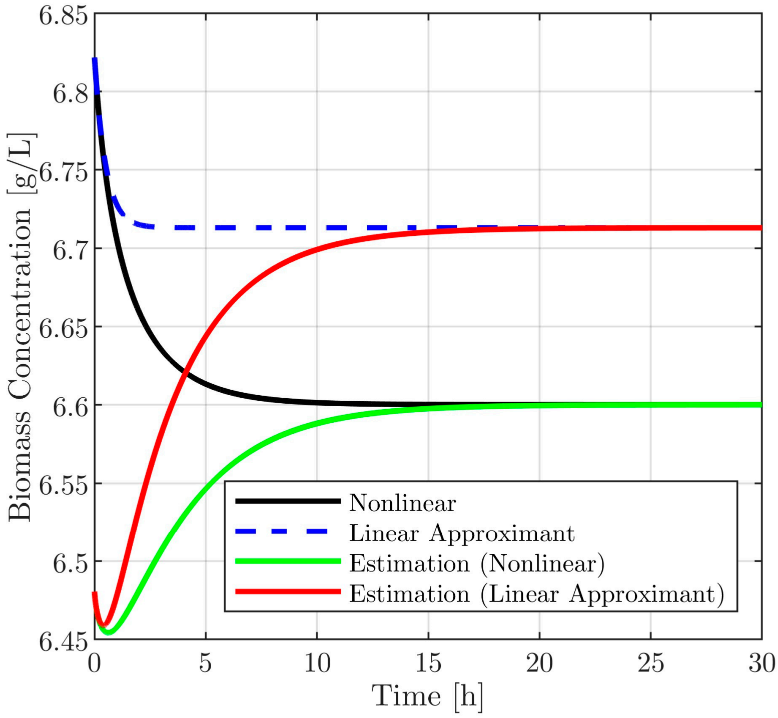

Figure A1. Biomass concentration estimation.

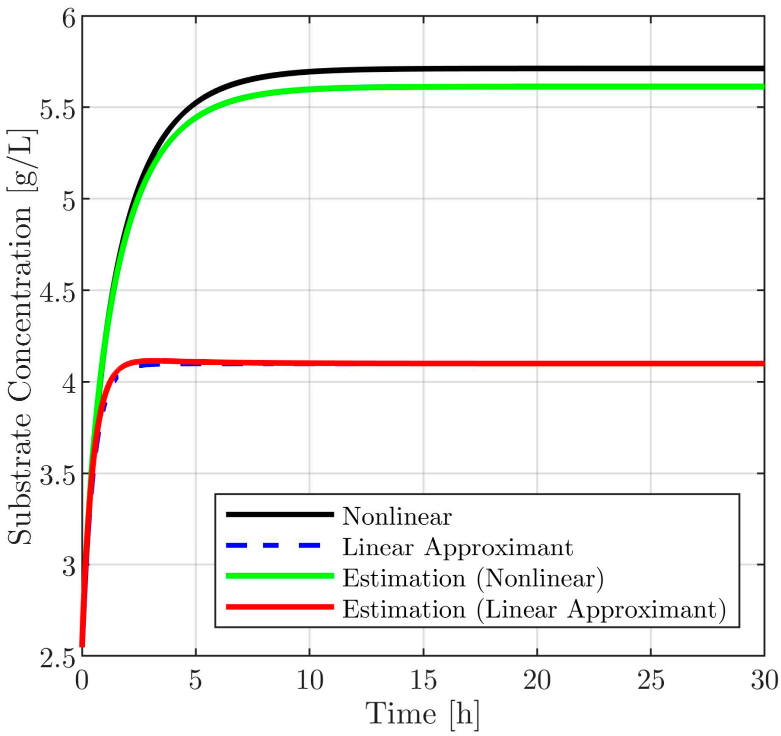

Figure A2. Substrate concentration estimation.

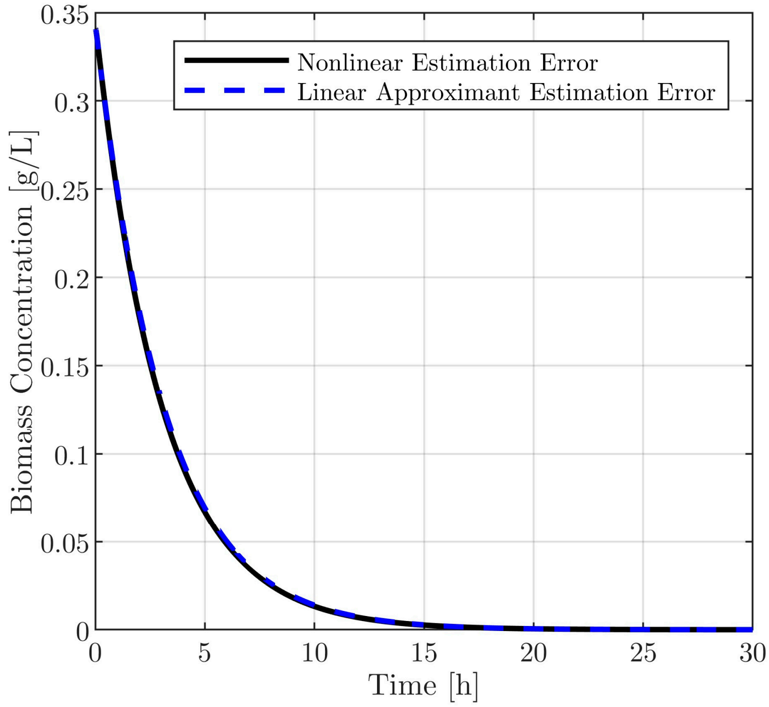

Figure A3. Biomass concentration estimation error.

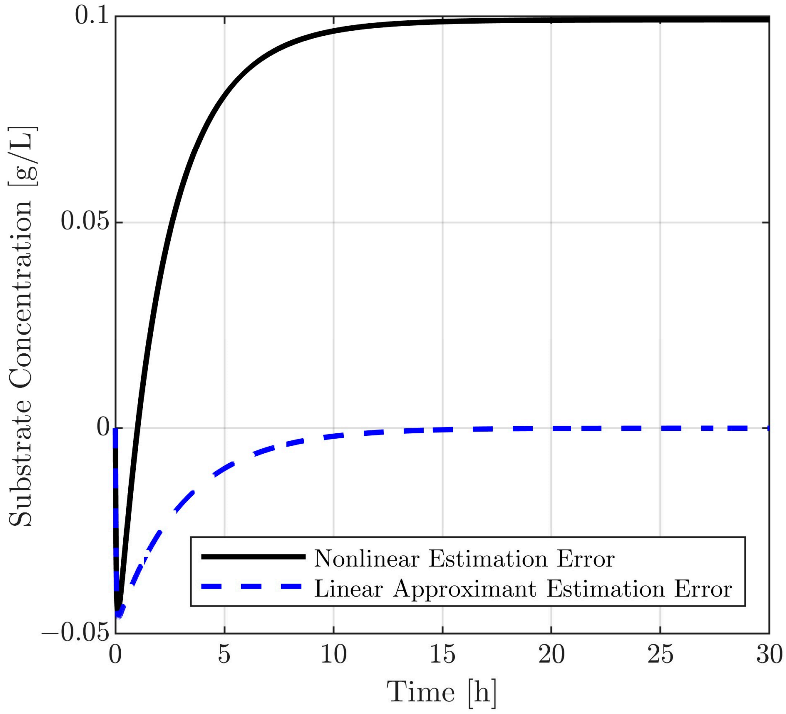

Figure A4. Substrate concentration estimation error.

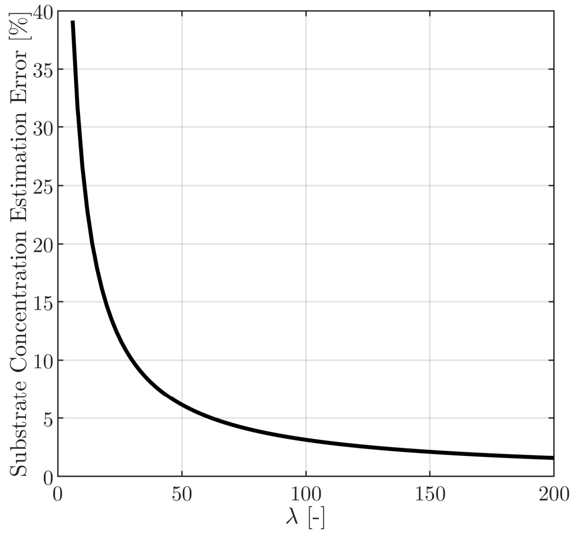

Figure A5. Substrate concentration estimation error vs. λ.

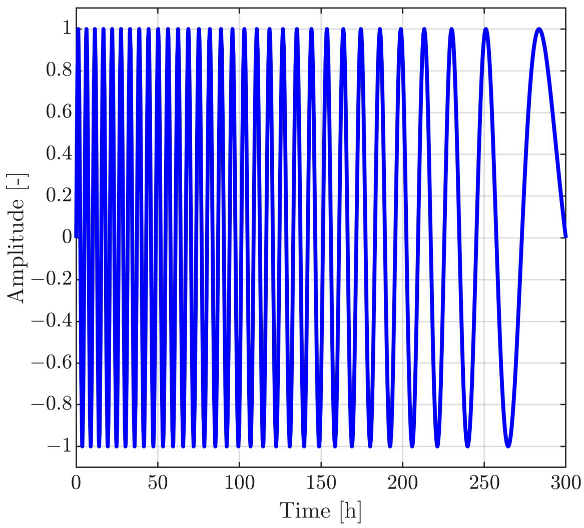

Figure A6. Chirp signal form.

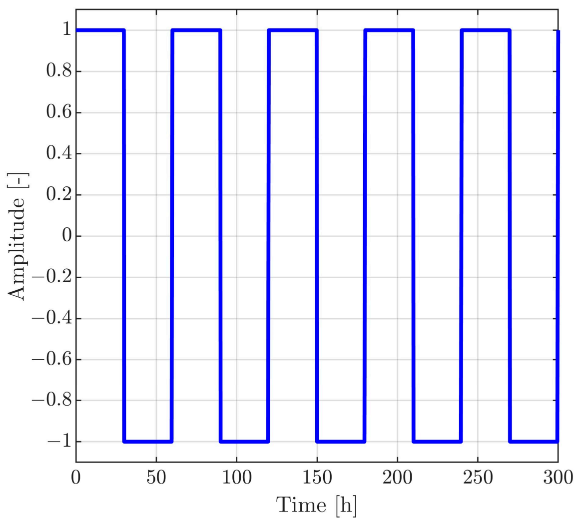

Figure A7. Pulse signal form.

Table A1. Identification of the linear approximant.

n/n	$\lambda_{O,i}$	$\lambda_{p,i}$	h_D	$\hat{h}_D$	h_N	$\hat{h}_N$	PF	MSE	FPE
1	0.0008930	0.0026790	68.760	68.731	99.974	99.970	99.933%	6.8930×10^{-12}	6.8931×10^{-12}
2	0.0008283	0.0024848	57.441	57.416	99.925	99.920	99.826%	5.6622×10^{-11}	5.6623×10^{-11}
3	0.0007734	0.0023203	50.064	50.041	99.884	99.877	99.749%	1.3502×10^{-10}	1.3502×10^{-10}
4	0.0007323	0.0021968	44.864	44.832	99.850	99.819	99.692%	2.2592×10^{-10}	2.2592×10^{-10}
5	0.0006911	0.0020734	39.948	39.926	99.811	99.794	99.635%	3.5680×10^{-10}	3.5681×10^{-10}
6	0.0006546	0.0019637	35.818	35.795	99.773	99.747	99.583%	5.1910×10^{-10}	5.1911×10^{-10}
7	0.0006180	0.0018540	31.914	31.923	99.729	99.798	99.532%	7.3435×10^{-10}	7.3436×10^{-10}
8	0.0005860	0.0017580	28.682	28.666	99.687	99.670	99.488%	9.7862×10^{-10}	9.7864×10^{-10}
9	0.0005540	0.0016620	25.623	25.624	99.640	99.684	99.443%	1.2934×10^{-9}	1.2934×10^{-9}
10	0.0005220	0.0015660	22.736	22.719	99.588	99.552	99.397%	1.7084×10^{-9}	1.7084×10^{-9}
11	0.0004946	0.0014837	20.399	20.393	99.537	99.547	99.359%	2.1451×10^{-9}	2.1452×10^{-9}
12	0.0004671	0.0014014	18.189	18.190	99.481	99.525	99.321%	2.6962×10^{-9}	2.6963×10^{-9}
13	0.0004397	0.0013191	16.105	16.099	99.417	99.420	99.281%	3.4144×10^{-9}	3.4145×10^{-9}
14	0.0004168	0.0012505	14.466	14.463	99.358	99.379	99.251%	4.1226×10^{-9}	4.1227×10^{-9}
15	0.0003940	0.0011820	12.914	12.901	99.291	99.230	99.219%	5.0136×10^{-9}	5.0137×10^{-9}
16	0.0003711	0.0011134	11.451	11.441	99.217	99.174	99.184%	6.1577×10^{-9}	6.1578×10^{-9}
17	0.0003483	0.0010448	10.075	10.073	99.133	99.154	99.154%	7.5082×10^{-9}	7.5083×10^{-9}
18	0.0003300	0.0009900	9.038	9.034	99.057	99.062	99.127%	8.9159×10^{-9}	8.9161×10^{-9}
19	0.0003117	0.0009351	8.057	8.051	98.972	98.947	99.103%	1.0533×10^{-8}	1.0534×10^{-8}
20	0.0002934	0.0008802	7.133	7.129	98.877	98.878	99.077%	1.2576×10^{-8}	1.2576×10^{-8}
21	0.0002751	0.0008254	6.264	6.261	98.769	98.759	99.049%	1.5155×10^{-8}	1.5155×10^{-8}
22	0.0002568	0.0007705	5.453	5.449	98.646	98.625	99.023%	1.8334×10^{-8}	1.8334×10^{-8}
23	0.0002431	0.0007294	4.881	4.878	98.541	98.526	99.002%	2.1292×10^{-8}	2.1293×10^{-8}
24	0.0002294	0.0006882	4.340	4.338	98.424	98.406	98.983%	2.4789×10^{-8}	2.4789×10^{-8}
25	0.0002157	0.0006471	3.832	3.830	98.292	98.284	98.961%	2.9195×10^{-8}	2.9196×10^{-8}
26	0.0002020	0.0006059	3.355	3.354	98.142	98.151	98.943%	3.4358×10^{-8}	3.4358×10^{-8}
27	0.0001883	0.0005648	2.910	2.908	97.971	97.968	98.919%	4.1220×10^{-8}	4.1221×10^{-8}
28	0.0001746	0.0005237	2.496	2.495	97.772	97.761	98.898%	4.9600×10^{-8}	4.9601×10^{-8}
29	0.0001654	0.0004962	2.238	2.236	97.621	97.594	98.882%	5.6621×10^{-8}	5.6622×10^{-8}
30	0.0001563	0.0004688	1.994	1.993	97.453	97.442	98.866%	6.4920×10^{-8}	6.4922×10^{-8}
31	0.0001471	0.0004414	1.764	1.763	97.263	97.241	98.851%	7.4750×10^{-8}	7.4752×10^{-8}
32	0.0001380	0.0004139	1.548	1.547	97.049	97.021	98.832%	8.7212×10^{-8}	8.7213×10^{-8}
33	0.0001288	0.0003865	1.346	1.345	96.804	96.788	98.812%	1.0255×10^{-7}	1.0256×10^{-7}
34	0.0001197	0.0003591	1.159	1.157	96.522	96.463	98.790%	1.2196×10^{-7}	1.2196×10^{-7}
35	0.0001106	0.0003317	0.985	0.984	96.193	96.150	98.776%	1.4440×10^{-7}	1.4440×10^{-7}
36	0.0001014	0.0003042	0.825	0.825	95.804	95.791	98.750%	1.7597×10^{-7}	1.7597×10^{-7}
37	0.0000923	0.0002768	0.680	0.679	95.339	95.309	98.722%	2.1747×10^{-7}	2.1747×10^{-7}

References

1. Koumboulis, F.N.; Fragkoulis, D.G.; Kouvakas, N.D.; Feidopiasti, A. Soft Sensor Design via Switching Observers. *Sensors* **2023**, *23*, 2114. [CrossRef]
2. Giannaris, G.L.; Kouvakas, N.D.; Koumboulis, F.N.; Vouyioukas, D. Switching Wireless Control for Longitudinal Quadrotor Maneuvers. *J. Intell. Robot. Syst.* **2021**, *102*, 42. [CrossRef]
3. Koumboulis, F.N.; King, R.E.; Stathaki, A. Logic-Based Switching Controllers–A Stepwise Safe Switching Approach. *Inf. Sci.* **2007**, *177*, 2736–2755. [CrossRef]
4. Economakos, C.E.; Koumboulis, F.N. A Safe Set Point Supervisor for MIMO Processes. In Proceedings of the 2006 IEEE Conference on Emerging Technologies and Factory Automation, Prague, Czech Republic, 20–22 September 2006.
5. Zefran, M.; Burdick, J.W. Design of switching controllers for systems with changing dynamics. In Proceedings of the 37th IEEE Conference on Decision and Control, Tampa, FL, USA, 16–18 December 1998.
6. Hespanha, J.P.; Morse, A.S. Switching between stabilizing controllers. *Automatica* **2002**, *38*, 1905–1917. [CrossRef]
7. Lam, S.; Davison, E.J. Control of plants with changing dynamics using switching model predictive control. In Proceedings of the 9th IASTED International Conference-Control and Applications, Montreal, QC, Canada, 30 May–1 June 2007.
8. Koumboulis, F.N.; Tzamtzi, M.P. A Metaheuristic Approach for Controller Design of Multivariable Processes. In Proceedings of the 12th IEEE Conference on Emerging Technologies and Factory Automation, Patras, Greece, 25–28 September 2007.
9. Koumboulis, F.N.; Tzamtzi, M.P. A generalised control metaheuristic framework for industrial processes. *Int. J. Autom. Control* **2010**, *4*, 218–233. [CrossRef]

10. Zentou, H.; Zainal Abidin, Z.; Yunus, R.; Awang Biak, D.R.; Abdullah Issa, M.; Yahaya Pudza, M. A New Model of Alcoholic Fermentation under a Byproduct Inhibitory Effect. *ACS Omega* **2021**, *6*, 4137–4146. [CrossRef]
11. Lin, Y.; Tanaka, S. Ethanol Fermentation from Biomass Resources: Current State and Prospects. *Appl. Microbiol. Biotechnol.* **2006**, *69*, 627–642. [CrossRef] [PubMed]
12. Bai, F.W.; Anderson, W.A.; Moo-Young, M. Ethanol Fermentation Technologies from Sugar and Starch Feedstocks. *Biotechnol. Adv.* **2008**, *26*, 89–105. [CrossRef] [PubMed]
13. Marín, M.R. Alcoholic Fermentation Modelling: Current State and Perspectives. *Am. J. Enol. Vitic.* **1999**, *50*, 166–178. [CrossRef]
14. Mantovanelli, I.C.; Rivera, E.C.; Da Costa, A.C.; Maciel Filho, R. Hybrid Neural Network Model of an Industrial Ethanol Fermentation Process Considering the Effect of Temperature. *Appl. Biochem. Biotechnol.* **2007**, *137*, 817–833. [PubMed]
15. Atala, D.I.; Costa, A.C.; Maciel, R.; Maugeri, F. Kinetics of Ethanol Fermentation with High Biomass Concentration Considering the Effect of Temperature. *Appl. Biochem. Biotechnol.* **2001**, *91*, 353–365. [CrossRef] [PubMed]
16. Kostov, G.; Popova, S.; Gochev, V.; Koprinkova-Hristova, P.; Angelov, M.; Georgieva, A. Modeling of Batch Alcohol Fermentation with Free and Immobilized Yeasts Saccharomyces Cerevisiae 46 EVD. *Biotechnol. Biotechnol. Equip.* **2012**, *26*, 3021–3030. [CrossRef]
17. Da Silva, F.L.H.; Rodrigues, M.I.; Maugeri, F. Dynamic Modelling, Simulation and Optimization of an Extractive Continuous Alcoholic Fermentation Process. *J. Chem. Technol. Biotechnol.* **1999**, *74*, 176–182. [CrossRef]
18. Da Costa, A.C.; Filho, R.M. Evaluation of Optimization Techniques for an Extractive Alcoholic Fermentation Process. *Appl. Biochem. Biotechnol.* **2004**, *114*, 485–496. [CrossRef]
19. Rivera, E.C.; Costa, A.C.; Atala, D.I.; Maugeri, F.; Maciel, M.R.W.; Maciel Filho, R. Evaluation of Optimization Techniques for Parameter Estimation: Application to Ethanol Fermentation Considering the Effect of Temperature. *Process Biochem.* **2006**, *41*, 1682–1687. [CrossRef]
20. Bartee, J.; Noll, P.; Axelrud, C.; Schweiger, C.; Sayyar-Rodsari, B. Industrial Application of Nonlinear Model Predictive Control Technology for Fuel Ethanol Fermentation Process. In Proceedings of the 2009 American Control Conference, St. Louis, MO, USA, 10–12 June 2009; pp. 2290–2294.
21. da Costa, M.A.V.; Normey-Rico, J.E. Modeling, Control and Optimization of Ethanol Fermentation Process. *IFAC Proc. Vol.* **2011**, *44*, 10609–10614. [CrossRef]
22. Costa, A.C.; Meleiro, L.A.d.C.; Maciel Filho, R. Non-Linear Predictive Control of an Extractive Alcoholic Fermentation Process. *Process Biochem.* **2002**, *38*, 743–750. [CrossRef]
23. Kabbaj, N.; Polit, M.; Dahhou, B.; Roux, G. Adaptive Observers based Fault Detection and Isolation for an Alcoholic Fermentation Process. In Proceedings of the 8th IEEE International Conference on Emerging Technologies and Factory Automation, Antibes-Juan les Pins, France, 15–18 October 2001.
24. Koumboulis, F.N.; Fragkoulis, D.G. Switching design for the observation of the biomass in alcoholic fermentation processes. In Proceedings of the 2017 XXVI International Conference on Information, Communication and Automation Technologies (ICAT), Sarajevo, Bosnia and Herzegovina, 26–28 October 2017.
25. Alvarado-Santos, E.; Mata-Machuca, J.L.; López-Pérez, P.A.; Garrido-Moctezuma, R.A.; Pérez-Guevara, F.; Aguilar-López, R. Comparative Analysis of a Family of Sliding Mode Observers under Real-Time Conditions for the Monitoring in the Bioethanol Production. *Fermentation* **2022**, *8*, 446. [CrossRef]
26. Petre, E.; Sendrescu, D.; Selişteanu, D.; Roman, M. Estimation Based Control Strategies for an Alcoholic Fermentation Process with Unknown Inputs. In Proceedings of the 2019 23rd International Conference on System Theory, Control and Computing (ICSTCC), Sinaia, Romania, 9–11 October 2019; IEEE: New York, NY, USA, 2019; pp. 224–229.
27. Selişteanu, D.; Petre, E.; Roman, M.; Ionete, C.; Popescu, D. Estimation Strategies for Kinetic Parameters of an Alcoholic Fermentation Bioprocess. In Proceedings of the SICE Annual Conference 2010, Taipei, Taiwan, 18–21 August 2010; IEEE: New York, NY, USA, 2010; pp. 3560–3565.
28. Selisteanu, D.; Marin, C.; Petre, E.; Sendrescu, D. Nonlinear Observers for the Estimation of Kinetic Parameters in an Alcoholic Fermentation Bioprocess. *Int. Rev. Autom. Control* **2011**, *4*, 124–132.
29. Roux, G.; Dahhou, B.; Queinnec, I.; Goma, G. *Software Sensor for Primary Metabolite Production Case of Alcoholic Fermentation*; LAAS Report 95187; Centre National de la Recherche Scientifique (CNRS): Paris, France, 1995.
30. Kamel, M.; Chaabane, M.; Chaari, A.; Farza, M. State and Unknown Input Observer Design for a Class of Non-Linear Systems: Application to a Fermentation Process. *IJSCC* **2011**, *3*, 34. [CrossRef]
31. Åström, K.J.; Wittenmark, B. *Adaptive Control*; Dover Publications: New York, NY, USA, 2013.
32. Sinha, N.K.; Rao, G.P. *Identification of Continuous-Time Systems: Linear and Robust Parameter Estimation*; CRC Press: Boca Raton, FL, USA, 2019.
33. Garnier, H.; Mensler, M.; Richard, A. Continuous-Time Model Identification from Sampled Data: Implementation Issues and Performance Evaluation. *Int. J. Control* **2003**, *76*, 1337–1357. [CrossRef]
34. Ljung, L. Experiments with Identification of Continuous Time Models. *IFAC Proc.* **2009**, *42*, 1175–1180. [CrossRef]
35. Young, P.; Jakeman, A. Refined Instrumental Variable Methods of Recursive Time-Series Analysis Part III. Extensions. *Int. J. Control* **1980**, *31*, 741–764. [CrossRef]
36. Drmač, Z.; Gugercin, S.; Beattie, C. Quadrature-Based Vector Fitting for Discretized H2 Approximation. *SIAM J. Sci. Comput.* **2015**, *37*, A625–A652. [CrossRef]

37. Ozdemir, A.A.; Gumussoy, S. Transfer Function Estimation in System Identification Toolbox via Vector Fitting. *IFAC-Pap.* **2017**, *50*, 6232–6237. [CrossRef]
38. Fontana, A.; Ghommidh, C.; Guiraud, J.P.; Navarro, J.M. Continuous Alcoholic Fermentation of Sucrose Using Flocculating Yeast. The Limits of Invertase Activity. *Biotechnol. Lett.* **1992**, *14*, 505–510. [CrossRef]
39. Gunawan, A.Y.; Sidarto, K.A. Washout and Non-Washout Solutions of a System Describing Microbial Fermentation Process under the Influence of Growth Inhibitions and Maximal Concentration of Yeast Cells. *Math. Biosci.* **2017**, *289*, 40–50.
40. *MATLAB*, version: 9.13.0 (R2022b); The MathWorks Inc.: Natick, MA, USA, 2022.
41. Henderson, D.; Jacobson, S.H.; Johnson, A.W. The theory and practice of simulated annealing. In *Handbook of Metaheuristics, International Series in Operations Research & Management Science*; Springer: Boston, MA, USA, 2003; Volume 57.
42. Delahaye, D.; Chaimatanan, S.; Mongeau, M. Simulated annealing: From basics to applications. In *Handbook of Metaheuristics. International Series in Operations Research & Management Science*; Springer: Cham, Switzerland, 2019; Volume 272.
43. Guilmeau, T.; Chouzenoux, E.; Elvira, V. Simulated Annealing: A Review and a New Scheme. In Proceedings of the 2021 IEEE Statistical Signal Processing Workshop (SSP), Rio de Janeiro, Brazil, 11–14 July 2021.
44. Sohail, A. Genetic algorithms in the fields of artificial intelligence and data sciences. *Ann. Data Sci.* **2023**, *10*, 1007–1018. [CrossRef]
45. Konak, A.; Coit, D.W.; Smith, A.E. Multi-objective optimization using genetic algorithms: A tutorial. *Reliab. Eng. Syst. Saf.* **2006**, *91*, 992–1007. [CrossRef]
46. Tabassum, M.; Kuruvilla, M. A genetic algorithm analysis towards optimization solutions. *Int. J. Digit. Inf. Wirel. Commun.* **2014**, *4*, 124–142. [CrossRef]
47. Aguilar-López, R.; Tec-Caamal, E.N.; Neria-González, M.I. Observer-Based Control for Uncertain Nonlinear Systems Applied to Continuous Biochemical Reactors. *Math. Probl. Eng.* **2020**, *2020*, 6417860. [CrossRef]
48. Pachauri, N.; Singh, V.; Rani, A. Two degree of freedom PID based inferential control of continuous bioreactor for ethanol production. *ISA Trans.* **2017**, *68*, 235–250. [CrossRef] [PubMed]